NUMERICAL SIMULATION OF ICE ACCRETION ON 3-D ROTOR BLADES

A Thesis
Presented to
The Academic Faculty

by

Eliya Wing

In Partial Fulfillment
of the Requirements for the Degree
Master of Science in the
School of Aerospace Engineering

Georgia Institute of Technology
May 2014

NUMERICAL SIMULATION OF ICE ACCRETION ON 3-D ROTOR BLADES

Approved by:

Dr. Lakshmi N. Sankar, Advisor
School of Aerospace Engineering
Georgia Institute of Technology

Dr. Daniel P. Schrage
School of Aerospace Engineering
Georgia Institute of Technology

Dr. Jechiel I. Jagoda
School of Aerospace Engineering
Georgia Institute of Technology

Date Approved: March 11, 2014

ACKNOWLEDGEMENTS

First and foremost, I praise God, my strength and my guide, for providing me this opportunity and granting me the capability to proceed successfully. I am grateful for the numerous people who have assisted me in completing this study.

I would like to thank my advisor, Dr. Lakshmi Sankar for his vision, guidance, and support. Through his abundant patience, I have gained an immense amount of invaluable knowledge and experience. I would also like to thank the members my committee, Dr. Schrage and Dr. Jagoda, for giving their time and valuable advice.

My gratitude also extends to my past and current labmates for their support and encouragement. I have really valued working with everyone and getting to know my labmates on a more personal level.

I sincerely thank my family and friends who have supported me in reaching this milestone. Without their encouragement, I would have never pursued or completed this graduate degree. I can't express enough gratitude and appreciation for their never ending support and love and always pushing me to go one step further.

TABLE OF CONTENTS

LIST OF TABLES

Page

LIST OF FIGURES

Page

LIST OF SYMBOLS

α	Non-dimensional volume fraction of water
β	Collection efficiency
β_f	Blade flapping angle
$\beta_0, \beta_{1c}, \beta_{1s}$	Flap angle coefficients
Δ	Incremental addition
ρ	Density
θ	Ice orientation angle
Ψ	Azimuth angle
N_{rev}	Number of revolutions
N_{Ψ}	Number of azimuth iterations
Ω	Angular velocity
A	Area
a_{∞}	Free stream speed of sound
c	Chord length
c_n	Normal force coefficient
c_p	Pressure coefficient
D	Distance
L’	Sectional lift
M	Mach speed
M_{roll}	Rolling Moment
M_{pitch}	Pitching Moment
r	radial position

R	Rotor radius
u_i	Non-dimensional velocity
U_∞	Free stream velocity
t	Ice thickness
T	Time
x, y, z	Cartesian coordinate system

Subscripts:

i, j	Cartesian direction
p	Referencing to perpendicular cutout
s	Referencing to streamline
w	Water

Superscripts:

n	Current iteration

LIST OF ABBREVIATIONS

AOA	Angle of Attack
AERTS	Adverse Environment Rotor Test Stand
CAA	Civil Aviation Authority
CFD	Computational Fluid Dynamics
CRREL	Cold Regions Research and Engineering Laboratory
CSD	Computation Structural Dynamics
FAA	Federal Aviation Administration
FAR/JAR	Federal/Joint Aviation Regulation
FIKI	Flight into known ice
FY	Fiscal year
HIC	Helicopter Icing Consortium
IFR	Instrument Flight Rules
IRT	Icing Research Tunnel
JAA	Joint Aviation Authority
LWC	Liquid Water Content
MVD	Median Volumetric Diameter
NASA	National Aeronautics and Space Administration
NTSB	National Transportation Safety Board
OAT	Outside Air Temperature
PFM	Power Force Model
RBF	Radial Basis Function
RPM	Revolutions per minute

SLD	Supercooled droplets
VLC	Vertical Lift Center

SUMMARY

Rotorcraft vehicles are highly sensitive to ice accretion. When ice forms on helicopter rotor blades, performance degradation ensues due to a loss of lift and a rise in drag. The presence of ice increases torque, power required, and rotor vibrations. The undesirable changes in the vehicle's performance have caused aviation regulatory bodies to require an intensive certification process for determining a helicopter’s airworthiness in icing conditions.

The two main categories of testing used to show certification compliance are flight testing and icing tunnel testing. Individually, flight tests and tunnel tests are unable to simulate all conditions required for certification forcing manufacturers to use an array of different testing methods. This increases the time, cost, and complexity of obtaining certification. In response, many rotorcraft manufacturers have chosen to not produce certified rotorcraft for icing conditions. However, the lack of certified rotorcraft have caused operational, and thus financial, consequences in both the commercial and military sectors. The evolving mission and performance requirements for modern day rotorcraft are making airworthiness during in-flight icing an essential design condition.

To alleviate the cost of ice testing, manufacturers depend on computational solvers to model ice growth and subsequent performance degradation. Computational solvers have the ability to evaluate a broader array of icing conditions in a safe and timely manner. However, this technology has limitations, requiring further exploration of methodology modifications to improve prediction accuracy.

One such area in need of investigation is the methodology behind simulating ice accretion for three dimensional bodies. Currently, most two dimensional ice accretion solvers use strip theory to generate ice growth along a three dimensional body such as a

wing or rotor blade. The shape is broken up into a series of two dimensional slices that are at constant $\frac{r}{R}$ or $\frac{y}{b}$ lines. Thus, ice growth is assumed to follow the direction of these perpendicular 2-D cutouts within this methodology. However, rotor blades can experience significant span-wise flow from separation or centrifugal forces. The migration of water droplets along the surface streamlines may cause ice to grow in an entirely different manner creating a larger build-up of ice at the wing or blade tip.

The focus of this document is twofold. First is an examination into the current state of icing certification for military and commercial helicopters. Results of this analysis discuss the consequences of in-flight icing and the difficulties associated with certification compliance techniques. Issues faced by manufacturers and operators suggest that methods alleviating the financial commitment to icing certification are paramount. Discovery of this need led to the second focus of this document, an inquiry into the ability of numerical methods to predict ice accretion. A major portion of this focus is dedicated to investigating the possible increase in prediction accuracy current icing methodology for three dimensional rotor blades is modified.

The new methodology incorporates the contributions of span-wise flow into LEWICE, a NASA 2-D ice accretion solver. Instead of obtaining flow-field characteristics along the constant $\frac{r}{R}$ blade cutouts, flow-field characteristics are calculated along a series of streamlines which span the entire rotor blade surface. Ice is then simulated to grow along the curved streamline trajectory.

Two test conditions were used to exercise the streamline ice accretion technique. The set of test conditions included variations in temperature, collective pitch, and span-wise strength. Comparison of the results to the classical strip theory approach indicate that the inclusion of span-wise flow had no signification effect on the overall ice shape.

CHAPTER 1

INTRODUCTION

1.1 Motivation

In-flight icing is considered to be one of the most dangerous weather hazards for aviation safety. Ice formation on the leading edge of lift producing surfaces will greatly reduce aircraft and rotorcraft efficiency by increasing weight, reducing lift, decreasing thrust, and increasing drag. Rotorcraft are especially susceptible to ice accretion and react to the presence of ice with more perilous consequences than their fixed wing counterparts. Due to its continuous threat to aviation safety, the US National Transportation Safety Board's (NTSB) has added in-flight icing to the "Most Wanted List" since 1997 [1].

In order to ensure aircrew safety during flight, regulatory bodies enforce a stringent in-flight icing certification process. Previously, compliance to certification rules was shown by completing a series of flight tests. Although multiple types of flight testing techniques exists, not all required weather systems are easily found in nature. It is also a costly and potentially dangerous process. In response to this, the Helicopter Icing Consortium (HIC) wanted to develop techniques for artificially testing the less common icing conditions. In the late 1980's, the HIC designed a two model testing program. The first experiment, completed in 1988, used an OH-58 tail rotor. The second, completed in the fall of 1989, used the "Power Force Model" (PFM). The PFM, shown in Figure 1a, was a one-sixth scale model of a UH-60 Black Hawk helicopter. An example of the ice accretion produced within the icing tunnel is provided in Figure 1b. The results of these two experiments demonstrated the viability of using a model rotor to obtain meaningful rotor icing accretion and performance data [2]. Since then, much progress has been made in

testing and modeling ice accretion and quantifying the effects of icing on the aerodynamic performance of lifting surfaces [3] [4] [5] [6] [7] [8] [9].

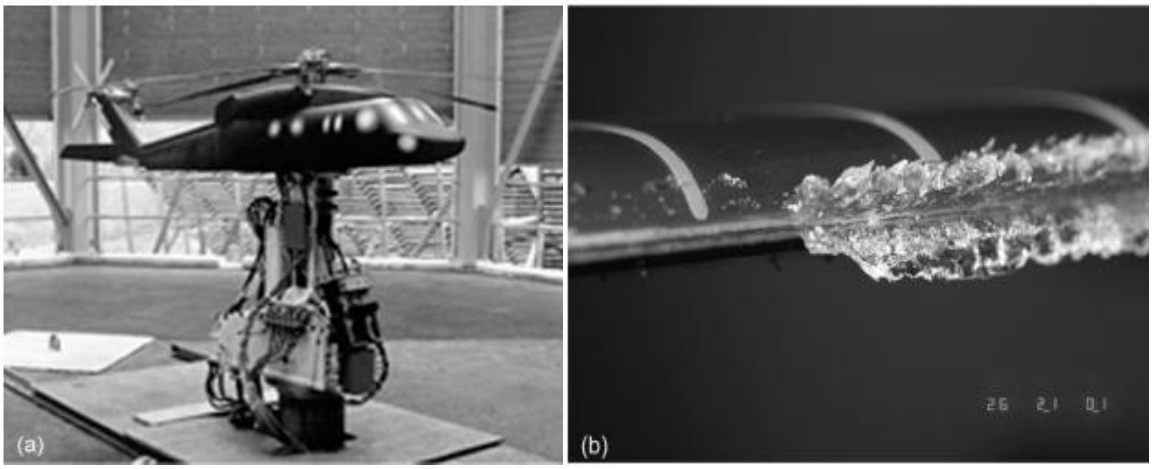

Figure 1: Images from the Power Force Model (PFM) test program in the NASA IRT 1986 [2]; (a) Scaled UH-60A Power Force Model (b) Glaze ice accretion on the main rotor

Even with the continuing advances in experimental testing with icing tunnels, testing remains very expensive and some conditions are still unattainable for flight testing and ice tunnel testing. As such, rotorcraft manufacturers and operators may choose to not undergo the complicated certification process. Instead, the rotorcraft community will tend to avoid the dangerous problem of ice accretion by restricting the flight envelope and limiting pilots to fly only in ice free environments. However, such methods impede mission operations in both the civilian and military sector. Passive methods of ice accretion prevention are not a practical or sustainable solution.

Numerical ice accretion solvers have the ability to investigate a much broader range of icing environments in a safe and efficient manner. Thus, incorporation of icing software in supplement to current compliance techniques can alleviate the stresses associated with obtaining certification. It is postulated that with the reduction in time and monetary commitment, rotorcraft manufacturers would be more inclined to certify their products for flight into known icing conditions. However, computational solvers are not without problems. As a result, investigations into new ways to improve the accuracy of computational ice accretion solvers are imperative.

1.2 Research Objectives

The work in this thesis addresses the current limitations in rotorcraft in-flight icing certification by formulating and implementing a new methodology for numerical predictions of ice accretion on three dimensional blades. The new methodology will include the presence of span-wise flow within a two dimensional computational solver. This modification is intended to increase ice prediction accuracy while still maintaining the computationally efficient process of using a two dimensional solver. The main goal of this thesis can be summarized by the two research objectives discussed below.

Objective 1: Critically analyze the state of in-flight icing certification for rotorcraft

Of particular interest throughout the course of this work is the real life applicability of numerical ice accretion solvers. Over the years, regulatory agencies have to create appropriate regulations and policies in order to protect aircrews from the known dangers of ice accretion. As a result of such rules, manufacturers wanting to design products safe for flight into known icing conditions must meet certain technical requirements. What is in question is not the legitimacy of said regulations, but the inclination of manufacturers to certify their products and the ease of obtaining icing certification. The goal of this objective is to identify any weaknesses within the current state in-flight icing. If any problems are discovered, it proves the relevancy for research focused on improving computational icing software.

Objective 2: Investigate the ice prediction accuracy with the incorporation of span-wise flow

LEWICE, NASA's ice accretion software, represents the accepted and accredited solver in the United States. Currently, ice prediction over three dimensional bodies is completed using a strip theory approach. Strip theory is a method that divides a 3-D body into a series of 2-D sections with constant cross sections in the span-wise direction. The

strip theory method has been validated with icing tunnel test experiments performed on rectangular wing sections [10]. However, strip theory neglects flow characteristics unique to three dimensional bodies. Specifically, swept wings and rotor blades are commonly subjected to the additional presence of span-wise flow. The migration of water droplets will no longer flow back along the constant $\frac{r}{R}$ blade cutouts, as assumed in the original strip theory approach. The aim of this objective is to modify the current methodology in order to incorporate the influence of the span-wise flow. Instead of obtaining flow-field characteristics along the constant $\frac{r}{R}$ blade cutouts, the flow-field characteristics are calculated along a series of streamlines which span the entire rotor blade surface. Thus, the LEWICE program will essentially be "tricked" into accreting ice along the curved streamline trajectory.

1.3 Organization of Thesis

The document is organized into six chapters. Starting with Chapter 2, a foundational overview of icing is provided. The chapter contains an introduction to the physics of ice accretion, current in-flight icing certification types, and a short linguistic review of the relevant terminology.

Chapter 3 discusses the multifaceted motivation behind the research effort. Here, the effects of in-flight icing on rotorcraft performance are examined. Further, the chapter will present an investigation focusing on the current practices of rotorcraft designers and operators to handle the dangers of ice accretion and the varying effectiveness of such practices. It is then argued that computation ice accretion solvers have the ability to alleviate the difficulties of completing certification compliance.

Chapter 4 provides an introduction to computationally predicting ice accretion. The chapter begins with a literature review of current computational icing solvers. Within the review, a general description of the each solver's functionality, different methodology techniques, and limitations are discussed. One particular solver, LEWICE, is expanded

upon and modified to simulate ice growth on airfoils. The resulting methodology is outlined and two validations cases are presented.

Building from the methodology given in Chapter 4, Chapter 5 modifies the technique and describes a new approach for ice prediction on three dimensional blades. The chapter begins by theorizing the importance of span-wise flow in ice accretion and lists the subsequent actions required to complete the task. The next section details the new modules within the methodology. The chapter ends by presenting the results of two test cases and assessing the relative differences in ice formation between the classical strip theory approach and the curved surface streamline based approach.

Finally, Chapter 6 concludes the thesis. This chapter summarizes this work and provides suggestions for future research.

CHAPTER 2

OVERVIEW OF IN-FLIGHT ICING

The purpose of this chapter is to provide background information essential to understanding the issues surrounding in-flight icing, i.e. the ice accretion process and relevant terminology of the field. A review of the icing environment and ice characteristics are first presented. The section then progresses onwards to a discussion about the different types of in-flight icing certifications for rotorcraft available by the United States, United Kingdom, and European regulatory bodies.

2.1 Formation of In-flight Icing

The development of in-flight icing is complex phenomenon which intertwines thermodynamics with aerodynamics. Essentially, ice will form on an aircraft's forward facing surfaces when it flies through moisture rich clouds at subfreezing temperatures. As the aircraft intercepts the liquid water droplets present in such clouds, the droplets either immediately freeze or become a mixture of liquid water and ice depending on the surrounding environment, e.g., the outside air temperature (OAT), pressure, density, water droplet diameter, and the liquid water content (LWC). LWC, synonymous with humidity, is a common parameter used to denote the amount of water contained within a volume of air. Other parameters which influence ice accretion are body geometry, Mach number, and time period of accretion.

Varying any one of the parameter listed above has the ability to change the resulting ice shape. To illustrate, Figure 2 is a representation of how ice accretion is affected by individual characteristics. Larger droplets, higher speeds, and thinner shapes will tend to increase the amount of ice accretion. A closer look into these trends exemplify the intricate

interactions of thermodynamics and aerodynamics. Specifically, the decreased formation of ice on blunter shapes in comparison to shapes with thin leading edges. For blunt bodies, air will tend to stagnate around the leading edge. The slowed air causes an increase in the ambient pressure and, in turn, an increase in temperature. Also, blunt bodies can have thicker boundary layers. The increased distance from the surface to the full ambient velocity provides more insulation between the skin and ice.

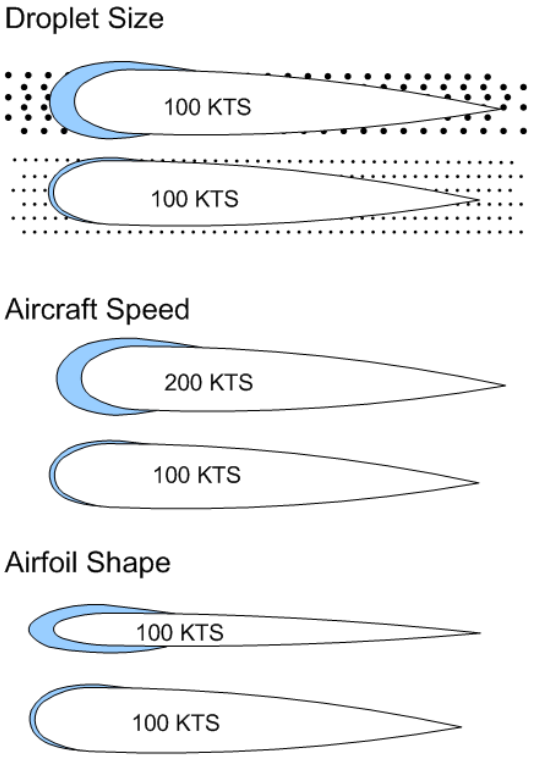

Figure 2: Illustration of how different characteristics influence the formation of ice [11]

2.1.1 Icing Environments

An icing environment is a description of the atmospheric conditions within a cloud. They are defined by the size and state of the cloud's water droplets, the droplets frequency of occurrence and spatial distribution, and several other ambient parameters. The United States' Federal Aviation Administration (FAA) has defined a set of categorize to classify certain combination of these parameters [12]. The main categories are as follows.

Supercooled Clouds

Supercooled clouds are clouds containing water droplets (below 32°F) that have remained in the liquid state. Such droplets will freeze upon impact and are referred to as supercooled droplets (SLD). Water droplets have been observed in the liquid state at ambient temperatures as low as -60°F.

Mixed Conditions

Mixed conditions are partially glaciated clouds at ambient temperatures below 32°F containing a mixture of ice crystals and supercooled water droplets.

Freezing Rain and Freezing Drizzle

Freezing rain and freezing drizzle occur when the precipitation existing within clouds or below clouds are at an ambient temperatures below 32°F with rain droplets remaining in the supercooled liquid state.

It is fairly recent that flight through supercooled clouds is necessary design conditions for the certification of rotorcraft. It comes as a response to the 1994 American Eagle ATR-72 crash in Roselawn, Indiana. The National Transportation Safety Board;s (NTSB) accident investigation report indicated the presence of droplet diameters much larger than those included in certification requirements at the time. Since then, the research community has put in significant effort to provide data characterizing the SLD environment [13].

Mixing conditions (i.e. the combination of ice crystals and SLD) and freezing rain/drizzle are currently not addressed in FAA Part 29 certification. Although not very common in nature, intercepting this environment during flight can present more severe icing conditions than those defined. There is a significant lack of data that has been

gathered on the effects of encountering mixed conditions. As such, all rotorcraft vehicles are not certified for operation in freezing rain or freezing drizzle [14].

2.1.2 Types of Ice Accretion

Significantly different ice shapes can result from various combinations of all the previously stated parameters, but there are only three main classifications of ice shapes, glaze ice, rime ice, and mixed ice.

Glaze Ice

Glaze ice is the result when droplets striking a surface have sufficient time to flow in a continuous film over the surface prior to freezing. It also commonly referenced to as “clear ice”. Glaze ice usually contains some air pockets resulting in a lumpy translucent appearance, although it can be smooth and clear. This type of ice is denser, harder, and at times more transparent than rime ice. Since a large portion of the surface was wetted prior to freezing, the glaze ice forms a very strong bond with the surface. Increasing droplet size will increase the likelihood of glaze ice formation.

Rime Ice

Rime ice forms due to the rapid freezing of SLD after they strike the surface. The rapid freezing traps the air causing the ice to be brittle and porous with an opaque appearance. Rime ice will typically form along the stagnation line of an airfoil. As seen in Figure 3, rime ice growth is more regular in shape and typically conforms more to the airfoil than glaze ice. The opacity of the ice makes it easier to pilots to visually detect.

Mixed Ice

Mixed ice is a combination of both glaze and rime ice. Clouds will commonly consist of a variety of droplet sizes. Mixed ice is formed when entering such an

environment and different droplet sizes strike the surface. Glaze ice formation is caused by large droplets and rime ice from small droplets.

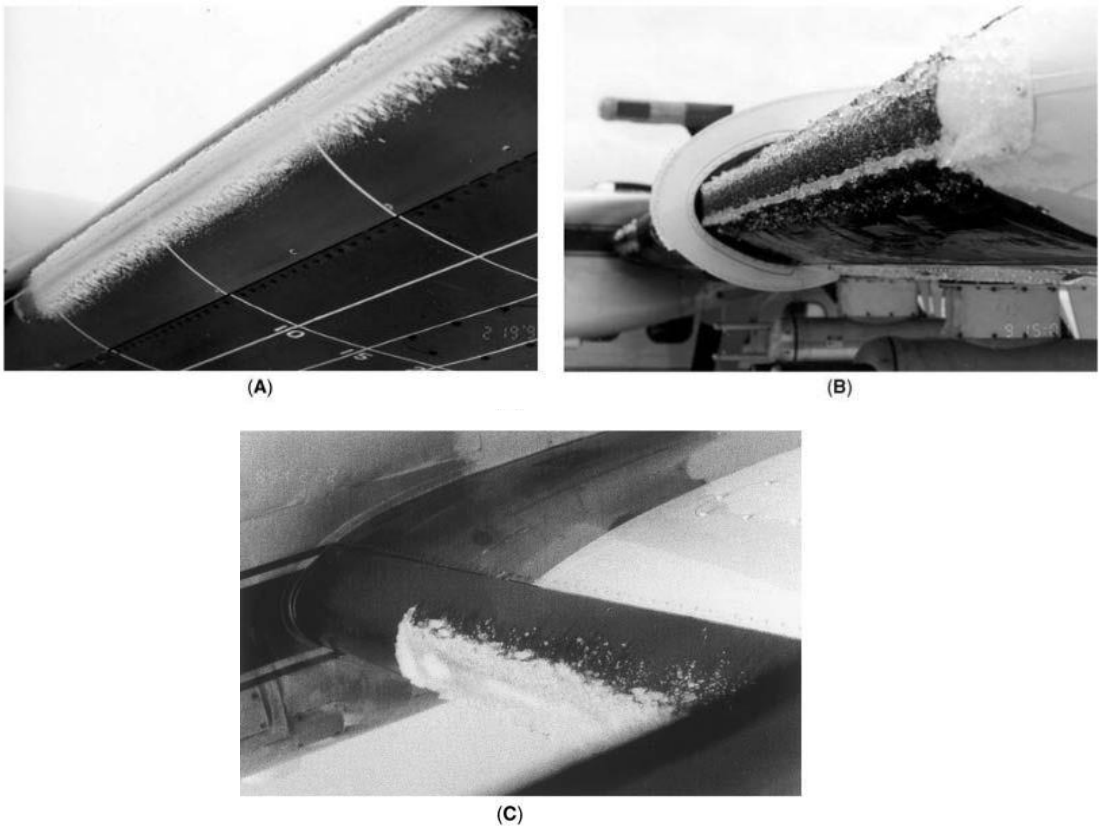

Figure 3: Post-flight photographs of ice accretion on the NASA Glenn Research Center's instrumented Twin Otter aircraft. The leading edge of the left wing is portrayed in each image: (A) rime ice, (B) glaze ice, (C) mixed ice [15]

2.2 Terminology for In-flight Icing Certification

2.2.1 FAA Operational Classification

There are several terms used operationally by flight crews to report the intensity of the encountered ice accretion to air craft control. Depending the severity of ice, the FAA recommends certain exiting procedures for pilots in order to preserve safe handling conditions of the aircraft [12]. They are as follows.

Light Icing

Light icing is the rate of ice growth which require occasional cycling of manual deicing systems to minimize ice accretion on the airframe. The provided reference rate is 1/4 inch to one inch per hour on the outer wing. The FAA recommends pilots experiencing this should consider exiting the condition.

Moderate Icing

Moderate icing is the rate of ice accretion which requires frequent cycling of manual deicing systems to minimize ice accretion ice accretion on the airframe. The provided reference is 1 to 3 inches per hour on the outer wing. Pilots experiencing this should consider exciting the condition as soon as possible.

Heavy Icing

Heavy icing is the rate of ice growth which requires maximum use of the ice-protection systems to minimize ice accretion on the airframe. The provided reference rate is more than 3 inches per hour on the outer wing. Pilots experiencing this should consider immediately exiting the condition.

Severe Icing

Severe icing is the rate of ice growth where ice protection systems are unable to remove the buildup of ice satisfactorily. Also at this accretion intensity, ice forms in locations not normally prone to icing, such as areas aft of protected surfaces and any other areas identified by the manufacturer. An immediate exit of this condition is required.

2.2.2 FAR/JAR Certification Levels

This section covers the current levels of icing certification for flight under US regulations (Federal Aviation Regulations or FAR), European regulations (Joint Aviation Regulations or JAR) and United Kingdom Regulations (Civil Aviation Authorities or

CAA). Between the regulatory bodies, there are three main types of icing certifications; zero icing, limited icing, and full icing. The objective of icing certification is to verify that throughout the approved envelope, a rotorcraft can operate safely in icing conditions expected to be encountered in service.

Zero Icing Clearance

Zero icing clearance covers that majority of commercial helicopters operating under JAR-29/FAR-29 airworthiness regulations [16] [14]. Operators must not deliberately encounter or route helicopters into areas of known in flight icing. Furthermore, if a helicopter inadvertently encounters icing, it must immediately leave the area. Most rotorcraft are not approved for flight in known icing (FIKI) conditions. For rotorcraft not approved for FIKI conditions, the FAA produces multiple safety advisories every year reminding pilots to expect icing any time when operating in visible moisture such as fog, rain, or clouds, and when the temperature is below 41°F. They state that pilots should be aware that icing is possible in these ambient conditions and should be prepare to leave the area of visible moisture or change to a warmer altitude as soon as possible [17].

Limited Icing Clearance

Limited icing clearance is a certification level awarded by the United Kingdoms (UK) Civil Aviation Authority (CAA) for flights within UK's airspace. Limited icing clearance approves flight in "a prescribed envelope in which the rotorcraft may be safely operated in icing conditions either for continuous periods or for a sufficient time to allow safe exit from the conditions, should this prove necessary" [18]. Limited icing clearances are only given by the CAA to specific operators which conduct agreed operations with particular aircraft. Helicopters are required to have ice-protection systems on the engine intakes, pitot tubes, and cockpit windows. They must also have some reliable means of measure ice-accretion rates. To obtain the clearance certification, the aircraft must be flown

in natural icing conditions to the same level of severity at which clearance is required. This is done to combine evidenced gained from test rigs and simulations with "real" data.

Full Icing Clearance

Full icing clearance allows helicopters to be flown in conditions described in Appendix C of JAR-29 or FAR-29 [16] [14]. These documents define the atmospheric envelope in which helicopters must be able to operate to receive a full icing clearance. The icing envelope is identical to the one used for certifying fixed wing aircraft. Helicopters must be able to hold in icing condition for 30 minutes at a destination. Full clearance requires helicopters to be outfitted with full ice protection on the main and tail rotors, the engine intakes, and stabilizer. To show compliance with certification restrictions, helicopters must complete an extensive matrix of icing tests. Since any one method cannot synthesize all necessary requirements, different forms of icing tests are required. Certification then becomes a very lengthy, difficult and expensive process.

CHAPTER 3

MOTIVATION FOR ICING RESEARCH

The purpose of this chapter is to discuss the multifaceted motivation behind conducting ice accretion research.

First, an overview of rotorcraft performance degradation in the presence of ice accretion is provided. This embodies the foundational concern for rotorcraft entering any icing environment. Next, the current practices of rotorcraft manufacturers and operators to overcome the dangers of in-flight icing are discussed. Currently, the rotorcraft community plays a very passive role in avoiding such dangers by not certifying most helicopters for flight into known icing conditions or through avoidance/cancelation of operations once an icing environment is detected. Subsequently, the next section is a synopsis of the known consequences stemming from such passive actions for civilian and military rotorcraft operators and the opinions of operators about the necessity of certification.

Although the consequences and opinions prove that more rotorcraft should be certified for some level of FIKI, an increase in demand by operators may not result in an increase in supply. Without a reduction in time, cost, and safety for manufacturers to complete the required compliance testing, creating icing certified products may still remain an impractical decision. Finally, it is argued that a heavier dependence on computational icing solvers to supplement testing will alleviate the burden of certification.

3.1 Consequences of In-flight Icing for Rotorcraft

In-flight icing is considered very dangerous weather hazard for aircraft and rotorcraft. The problems caused by ice accretion stem from the presence of ice forming on lifting surfaces. Wing, rotor, and tail ice accretion can result in significant reduction of aerodynamic

performance. When ice forms around the leading edge of an airfoil, the changing shape and surface roughness greatly affects the acceleration of the flow leading to a loss of lift and rise in drag. Ice accretion can also influence premature flow separation downstream of the ice shape giving rise to stall at considerably lower angles of attack.

While icing affects fixed-wing and rotorcraft vehicles alike, rotorcraft are more susceptible to ice accretion and are predisposed to various complications that are not common to fixed wing aircraft. Such consequences are caused by the design characteristics unique to rotorcraft.

In comparison to fixed wing aircraft, helicopters operate at much lower conditions, typically flying at cruise altitudes between 1,000 and 10,000 ft. At such altitudes, rotorcraft vehicles are more likely to encounter icing environments as large liquid water content can be expected at ambient temperatures between -22°F and 22°F. The higher LWC level may create icing environments such as freezing drizzle and freezing rain. When these droplets contact the rotorcraft surface, ice will likely form.

In most helicopters, the main rotor disc is sole method of generating lift, maneuverability, and forward momentum. When ice forms on helicopter rotor blades, performance degradation ensues due to the aforementioned loss in lift and rise in drag. The presence of ice increases torque, power required, which further lead to increased rotor vibrations [2]. For helicopters, the loss of lift equates to a decrease in pitch angle limits, much like a decrease in stall angle limits for fixed wing aircraft. The reduction in pitch angles narrows the operational envelope as trimmed steady level flight becomes less achievable. This will subsequently restrict the allowable gross weight, forward speed, and altitude of operations.

Shedding of ice during flight is another common occurrence with significant consequences. For rotorcraft, combining high rotor speeds and centrifugal forces may forces strong enough to break the bond between the ice and blade surface. Asymmetric ice shedding (affecting fewer than all of the blades) can cause extreme vibrations depending

on the amount of ice discharged, the type of rotor systems, and other factors. The dislodged ice may potentially strike the fuselage, creating airframe damage, or be ingested by the engine causing engine damage or failures.

The degradation of autorotational qualities is another icing consequence unique to helicopters [19]. Autorotation refers to the descending maneuver where a helicopter must land with its engine disengaged from the main rotor system. With the rotor completely unpowered, blades are driven by the upward flow of air through the rotor. In icing, the deterioration of normal autorotational limits are the result of ice accumulating in greater amounts near the inner portion of the rotor disk. As the air flows up through the disk, the presence of ice at the blade root directly decreases blade efficiency during autorotation. Also, the increased weight from the ice forces higher rates of decent and unstable rotor RPM. Specific autorotation properties are required for certification to ensure a safe and controlled landing. Any reduction of such properties poses a serious threat to safe helicopter operations.

Finally, helicopter pilots have a harder time detecting the rate of ice growth than their fixed wing colleagues. One of the main methods for gauging the severity of ice is through visual cues such as ice buildup on the windshield or other visible surface sections. Due to the rotor's angular velocity, icing accretes at an accelerated rate on the rotor blade compared to the fuselage. Thus, in order to judge the severity of icing, helicopter pilots require more cues than just a visual determination based on nearby surfaces. All in all, helicopter have a distinct and arguably more dangerous disadvantage with ice accretion on lifting surfaces.

3.2 Current Practices of Rotorcraft Designers and Operators

Many manufacturers believe the additional benefits stemming from a larger operational envelope do not overcome the cost of certification. This has created a rotorcraft community where most helicopters are simply not certified to fly into known icing conditions. In fact,

it was mentioned briefly in a 2002 US Army report that the UH-60A Blackhawk and AH-64A Apache were the only US military helicopters certified for full icing clearance [20]. For another example of how uncommon it is for helicopters to have full icing certification, out of the entire Canadian fleet of IFR passenger-carrying aircraft in 2007, only five civil de-iced rotorcraft were operating in the country [21].

In other words, helicopter manufacturers and operators have coped with the difficultly of obtaining certification and the dangers of ice accretion by taking a very passive route and avoiding in-flight icing altogether.

In 1998, the European Commission funded a project to critically analyze the current certification and operational regulations, entitled the European Research on Aircraft Ice Certification (EURICE) [22]. The project interviewed several organizations which design, certify, or operate helicopters in Canada or Europe. The EURICE authors noted the same lack of certified helicopters, even for operations that frequently encountered icing conditions.

3.3 Consequences of Passive Flight Avoidance Actions

The intent of this section is to discuss the two main consequences caused by passively avoiding certification. First, flight crews are too constrained by the allowable operating envelope and do not adhere to required regulations. Second, avoiding FIKI has significant consequences to day to day operations.

3.3.1 Disregard of Certification Regulations

There are claims that helicopter pilots will still fly into icing conditions even though they lack certification. When company pressures increase, operators and aircrews will fly for brief periods in icing conditions in order to maintain the schedule of operations. Some of the interviewed aircrews stated “we know the helicopter can cope with limited icing

conditions because we have done it and we've spoken to other crews who have also flown icing".

Unfortunately, the confidence of maintaining controlled flight is misplaced. Referring a review of U.S. icing related aircraft accidents from 1978 to 2002, multiple fixed wing pilots involved with icing accidents got into a situation the aircraft could not handle by believing that flying for only a couple of minutes to pass through the icing cloud would not be a problem, only to find themselves with considerable ice after a very short encounter [23]. The pilots expressed that they were often surprised by the speed of ice accretion and caught off guard. This pattern in fixed wing pilots and the EURICE operators seem to indicate a common and misguided expectation that hazards can be simply avoided by passing quickly through icing environments.

EURICE investigators were under the impression that as long as no incidents or accidents occur, the operators will continue to fly for short periods of time in icing without clearance. Thus, the decision to not certify helicopters in hopes of providing complete protecting of aircrews and operators from the dangers of ice accretion can therefore be consider insufficient.

3.3.2 Obstruction of Operations

For pilots that choose to abide by rotorcraft regulations, the restriction of allowable operating environments greatly affects operations. The US Army's Cold Regions Research and Engineering Laboratory (CRREL) conducted an extensive survey of aviation commanders worldwide to assess what effect icing had on military operations from FY2001 to FY2002 [20]. At the time of this study, the army believed the icing did not "negatively affect their mission" since there are no icing accidents or safety related issues. However, the military neglected to consider that not being able to conduct aviation operations under all or most icing conditions will significantly alter the army commander's options for mission success. If icing deprives a commander of even part of his or her

aviation assets for any of the roles listed above, from attack to evacuation, then the mission has been affected.

CRREL found that icing does indeed cause mission cancellations and abortions because of forecast or actual in-flight icing. The conducted survey consisting of several questions pertaining to what problems, if any, are encountered with ground icing and in-flight icing.

One such question asked commanders if a significant number of flights were canceled as a result of either ground or in-flight icing. CRREL rated that if at least 50% of the commanders cited the effect on mission accomplishment as moderate or high then the effect can be considered serious problem. By the 50% criterion, forecasted icing conditions in the flight plan have a significant impact on mission accomplishment in Belgium, Germany, and Korea, at Forts Drum, Wainwright, Belvoir, and Eustis, and in Indiana. SHAPE (Belgium) aircraft, which fly weekly to Germany and the United Kingdom, will encounter light to moderate icing on almost every mission during the winter period and occasionally high-altitude unforecasted icing.

Another question addressed the frequency of canceled scheduled flights as a result of actual or forecast icing and the frequency of disrupted flights (aborted, redirected, etc.) as a result of unexpected in-flight icing. The scale for assessing icing's impact in a given month is as follows: no impact (flights never affected), moderate impact (1–10% of flights affected), and severe impact (more than 10% of flights affected).

Applying this criterion, CREEL reported that the majority of units in Korea, Germany, and at Fort Campbell experience at least a moderate impact on mission as a result of actual or forecast icing. Units in Belgium, Illinois, and at Fort Wainwright also experience a moderate impact on mission. Severely affected units are in Germany, Indiana, and Minnesota, and at Forts Drum and Eustis. In other words, all surveyed units experienced at least moderate impact from flight cancellation.

For the frequency of disrupted flights, flight disruption is a severe problem (more than 10% of scheduled flights affected) only for the one of the surveyed units located in Katterback, Germany. In December, January, and February, 11–25% of this unit's flights are disrupted as a result of unexpected in-flight icing. For the majority of units (62%), more flights are canceled in midwinter as a result of actual or forecast icing than are disrupted by in-flight icing.

In addition to the questionnaire, CREEL analyzed the recorded accidents and incidents caused by icing. Out of the 255 reported icing adverse events, 160 occurred in flight and the remaining 95 occurred on the ground. A common in-flight icing accident in helicopters was damage to a whip antenna. For example, one helicopter reported the following: “During instrument approach into Grafenwohr AAF, aircraft entered moderate icing condition. Ice accumulated on no heated surfaces. Suspected that ice accumulated on the whip antenna causing antenna to flex and eventually fracturing and fraying the antenna”. Severe incidents or accidents from in-flight icing are usually not a common occurrence.

To conclude, a surface level inquiry based on accident and incident reports will suggest that in-flight icing is not a significant problem. CREEL found that icing related incidents are common, but only typically resulted in minor structural damages. However, through their investigation, it was discovered that US Army operations are frequently obstructed due to the presence of icing conditions. The inability to fly through such environments requires the Army to cancel scheduled flights. Thus, avoiding in-flight icing severely hinders mission accomplishment.

3.4 Recommendations Made by Operators

It is also important to review the opinions expressed by those who are forced to deal with every day consequences of not having the proper rating of in-flight icing clearance. Operators in the EURICE study stated they would like the manufacturers to certify all

helicopters for limited icing. With limited icing certification, relevant information, such as permitted engine torque rise and escape procedures, could then be provided to pilots who fly into icing conditions. Currently, pilots who fly in helicopters without an icing clearance only learn about problems with handling from other pilots and company internal communications. A further advantage of a limited icing clearance is that it allows helicopters to takeoff and climb through icing cloud at low altitudes, into conditions free of icing, or with limited icing [22].

For the particular needs of the operators in the EURICE survey (flight operations to off shore oil rigs), full icing clearance were considered unnecessary because the price of full icing clearances is greater than the expansion of the operational envelope. Operators did say that they commonly had difficulty in finding escape routes for limited icing clearances which would not be an issue with full clearance helicopters.

US Army commanders expressed a desire for more helicopters with icing certification. Multiple respondents of the CRREL survey noted that Chinook helicopters would greatly benefit from having icing certification. One pilot who has flown Chinook helicopters in Italy, Korea, Alaska, and throughout the US commented that moderate icing builds up quickly and can be very disconcerting without deicing capability [20].

3.5 Problems with Current Certification Compliance Techniques

One of the main hindrances for manufactures attempting to obtain limited or full icing clearances is the cost of testing. Presently, helicopter icing certification is a lengthy, expensive, and a potentially dangerous process. Aircraft and rotor industries mainly rely on two testing methods to determine the aerodynamic performance due to icing; flight testing and wind tunnel testing. Current procedures for icing certification put emphasis on performing helicopter flight tests over a wide range of natural icing conditions for accuracy purposes. For example, the CAA requires natural ice flight testing for limited icing clearance to demonstrate compliance with regulations. Natural icing tests are a type of

flight test which require aircrews to fly in appropriate weather condition found in nature and illustrate proper de-icing/performance capabilities.

Natural icing tests are considered to be the most difficult and most dangerous method of demonstrating regulatory compliance. This type of testing is challenging because the required weather conditions do not happen often in nature and thus force manufactures to bend to the whim of weather systems. Another potential problem is when the forecasted icing systems dissipates before the rotorcraft reaches the cloud, or the conditions (temperature, wind speed, etc.) may fluctuate before or during testing thus nullifying the testing attempt.

All types of flight testing are inherently dangerous because of the aforementioned performance degradation due to ice growth. There is always a risk that the electrothermal systems may not handle the icing environment as designed thereby putting the aircrew in harm's way. If allowable, wind tunnel testing provides a safer and more predictable alternative. Tunnels provide more control over the atmospheric conditions and remove flight crews from the equation. However, not all required conditions can be simulated in tunnels, and cost and accuracy remain a problem for rotorcraft manufacturers.

3.6 Contributions of Computational Ice Prediction Codes

Due to in-flight testing hazards, high testing cost, and unattainable atmospheric conditions aircraft and rotorcraft companies have begun to depend on computational ice accretion solvers to reduce the amount of required flight and tunnel testing. Computational solvers have the ability to safely and more efficiently predict ice shapes for far more flight conditions than previously possible. Pretest predictions of the ice shape can pinpoint the most critical icing conditions and the resulting performance/handling qualities. Thus, computational solvers are advantageous for manufacturer use in obtaining certification and for designer use in creating next generation ice protection technologies.

This is not to say that ice prediction codes are the immediate key to all success. There are several codes available in the public and private domain and all have weaknesses in one area or another [24] [25] [26] [27]. Due to the complexity surrounding the physics of ice growth, codes incorporate empirical data or equivalent measures to calculate important parameters. This can degrade the accuracy of ice shape predictions. As an example, LEWICE, the US industry standard code written by NASA, typically provide inaccurate results in the prediction of ice shapes under glaze ice conditions. However, rime ice shapes have been well documented to match with experimental data. Further research is required to improve the accuracy and robustness of computational simulations.

Thus, it can be concluded that research focused on improving simulation fidelity of computational ice accretion is largely beneficial to the rotorcraft community. To put it more simply, the availability of more accurate predictions will persuade manufacturers to increase their dependency of icing codes to supplement certification testing.

One of the main reasons for manufacturers to design rotorcraft for zero icing clearance is not from a lack of customer interest, but due to the cost of certification. It is theorized that if more helicopters are certified for flight into known icing conditions, safety and operational success would increase as missions are no longer grounded or rerouted due to adverse weather.

CHAPTER 4

NUMERICAL SIMULATION OF ICE ACCRETION

The intent of this chapter is to introduce the numerical simulation of ice accretion. First presented is a literature review focused on some of the better known computational ice accretion programs. The purpose of this review is to provide a foundational understanding of the simulation process and some of the current techniques available. Common limitations are also discussed.

The chapter then describes a modification to the existing LEWICE framework to predict ice growth on two dimensional shapes. The last section presents two LEWICE validation cases for a NACA0012 airfoil. The results are compared to two sets of experimental data, a 1991 icing experiment conducted by Britton and Bond and an icing experiment conducted by the Pennsylvania State University's Vertical Lift Center of Excellence.

4.1 Literature review of Icing Simulation Programs

A number of ice accretion models are available in the public domain and as add-on packages to commercial computational fluid dynamics (CFD) software. There are several methods used to compute ice accretion, but all consist of the four distinct modules illustrated in Figure 4; (1) flow field calculation, (2) water droplet impingement characteristics, (3) thermodynamics of ice accretion, and (4) calculation of resulting ice shapes. Programs may use a 2-D or quasi-3-D inviscid flow code (Panel method) to obtain the flow field or use a Navier-Stokes solver to capture unsteady effects. Particle tracking techniques for collection efficiency calculations are found with Lagrangian or Eulerian methods. Most ice accretion solvers incorporate a 1-D mass and heat transfer balance at

the surface to predict ice shapes. Some of the better known ice accretion codes are NASA's LEWICE [28], ONERA3D [25], FENSAP-ICE [26], and Bombardier Aerospace's CANICE [27].

Figure 4: The four distinct modules incorporated within ice accretion solvers

Several of these ice accretion tools will be discussed in more detail in the following sections. It is important to acknowledge that each icing software has multiple versions available with additional capabilities. For simplicity, only the baseline code is described in this literature review.

4.1.1 LEWICE

LEWICE, created by the NASA Glenn Research Center, represents the currently accepted and accredited approach in the United States. The computer software contains an analytical ice accretion model that evaluates the thermodynamics of the freezing process that occurs when supercooled droplets impinge on a body. It is a two-dimensional or three dimensional solver that uses the input model geometry, flight conditions, and icing conditions to calculate the amount of ice, its location on the surface, and the shape of the ice. LEWICE uses a potential flow solver, a Lagrangian droplet trajectory analysis, and a mass and energy balance for the determination of ice growth [28]. The panel method, developed by Hess and Smith [29], uses distributed sources, sinks, and/or vortices to describe the flow field about a body being modeled by a series of line segments. The droplet trajectory analysis is based the work by Frost, Chang, Shieh, and Kimble [30]. LEWICE modifies the droplet analysis method by assuming spherical particles and neglecting gravity forces. An integral boundary layer formation is then used to determine the skin

friction, local heat transfer coefficient and near-body flow characteristics. Finally, it uses a modified Messigner model for ice accretion thermodynamic analysis [31].

The popularity of LEWICE stems from its extensive validation using a large database of experimental ice shapes. Figure 5 illustrates an example of one such validation case. The ice shape predicted with LEWICE directly matches that of the icing experiment. In addition, the calculated local collection efficiency values were compared to test results conducted in NASA's Icing Research Tunnel (IRT) [24].

However, the software is not flawless. Surface roughness is seen to strongly influence the local heat transfer processes. LEWICE uses an equivalent roughness concept which models the actual surface roughness by an average value which yields the same heat transfer characteristics. This method is widely recognized as a weak point in the analysis.

LEWICE also has difficulty predicting glaze ice shapes. Figure 6 illustrates this limitation. The image shown compares a LEWICE prediction (blue lines) to experimental data (pink lines). The multiple blue lines represent the build-up of ice thickness at each computational time step. The calculated ice shape misses the ice horns located on the lower surface and places the upper ice horn at a lower angle in comparison to the experimental data. The inaccuracies in glaze shape predictions are due to the increased sensitivity of the local heat and mass transfer on the surface since droplets will only partially freeze on impact. The complexity of predicting heat transfer coefficients, as well as local surface roughness values, have led to several empirical and approximate methods which have several shortcomings.

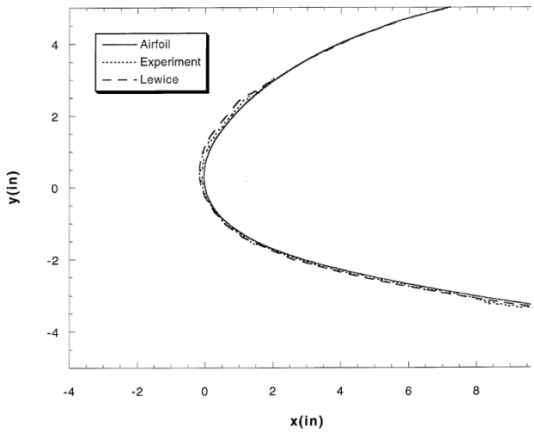

Figure 5: Rime ice prediction is in agreement with experimental data [24]

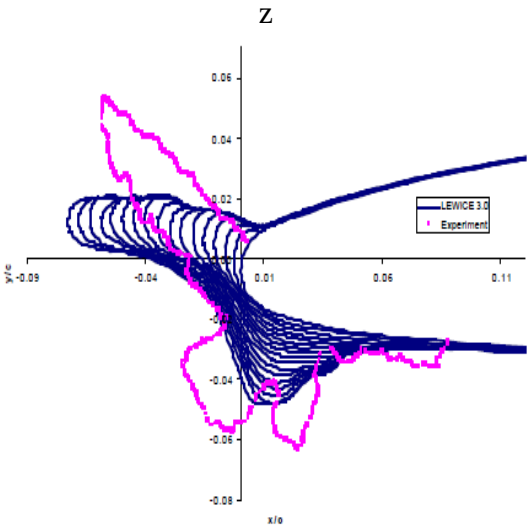

Figure 6: Glaze ice prediction misses lower surface ice horns and angle of top horn [28]

4.1.2 FENSAP

An alternative to LEWICE's Lagrangian particle tracking for droplet trajectory calculations is the Eulerian based method used in codes such as FENSPAP-ICE. FENSAP-ICE calculates the ice accretion on two or three-dimensional geometries. The program is built in a modular fashion to solve each flow, impingement, and accretion via field models based on partial differential equations. Much like LEWICE, this simulation works in four steps. First, FENSAP-ICE accepts the flow field from any Navier-Stokes CFD analysis chosen by the user. It then uses an Eulerian approach to compute the collection efficiency. Next, the code solves the mass balance and heat transfer equations at the airfoil surface in a time dependent manner. Finally, it solves a conjugate heat transfer problem with an anti-icing heat flux (if an anti-icing system is present) [32]. The main strength of the new method compared to other icing codes is the possibility to use advances from other computational fluid dynamics areas were partial differential equations are used.

FENSAP-ICE validation results show good agreement with other code calculation results for geometries available in the open literature. Figure 7 is a comparison of FENSAP-

ICE (denoted as ICE3D on the figure) to LEWICE. The multiple solid black lines represent the ice build-up at each time step. The ICE3D ice shape matches that predicted by LEWICE's. However, FENSAP-ICE suffers the same weakness as LEWICE in its difficulty to accurately predict glaze ice accretion (seen in Figure 8).

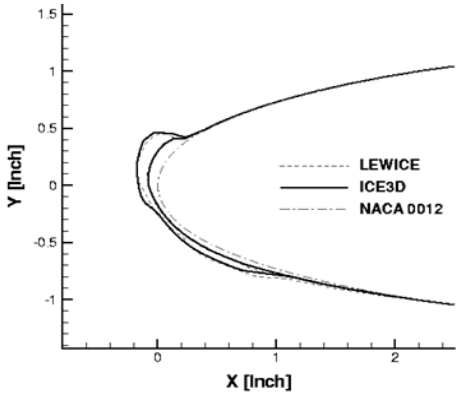

Figure 7: Rime Ice agreement with LEWICE software

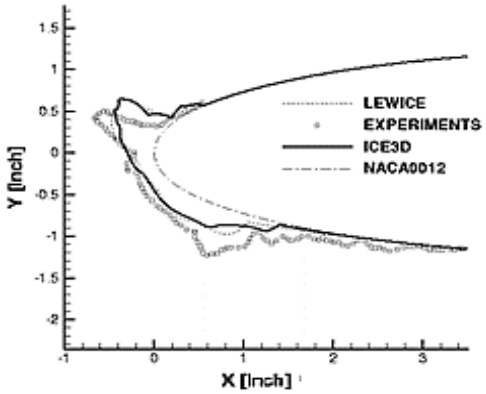

Figure 8: Incorrect prediction of glaze ice shape

4.1.3 CANICE

Icing/anti-icing simulation code CANICE is one of the four major icing simulation codes previously mentioned at the start of this chapter. It is used for the certification of Bombardier aircraft in icing conditions. Like other ice accretion tools, CANICE consists of four distinct modules: (1) the flow field, (2) water-droplet impingement characteristics, (3) thermodynamics of ice accretion, and (4) the resulting ice shape and/or runback.

The program utilizes the aerodynamic panel method to solve for the potential flow which is then corrected for compressibility effects. The code uses Lagrangian tracking to determine droplet trajectories and impingement locations. Calculation of thermodynamic principles are computed with a modified Messinger model in conjunction with an integral boundary-layer solution for heat and mass transfer rates. The code includes roughness, runback, and water splash/ice shed subroutines based on water-bead model.

To solve for the ice accretion, CANICE employs a quasi-steady approach. With this method, the flow field is re-computed at each time step to determine the ice growth as time proceeds. CANICE validation cases show good results for rime ice conditions. As

mentioned before, the algorithms enlisted in icing programs such as LEWICE and FENSAP-ICE can become unreliable when the complexity of the ice formed on the surface increases, as is the case of glaze ice. It attempts to improve the ice simulation by employing a 3-D viscous-inviscid interaction technique within a thermodynamic analysis module. However, this approach is very time-consuming and is not recommended [27].

There are some problems and limitations with CANICE. The code tends to predict excessive runback especially near the front stagnation region. As a consequence, either unusually large ice horns form outside the stagnation region or ice is seen to form well behind the impingement limits. It also has difficulty accurately modeling the surface roughness and heat transfer coefficient values. Figure 9 illustrates several CANICE results for glaze ice prediction. The general shape predicated matches reasonably with the experimental data, but inconsistencies still remain.

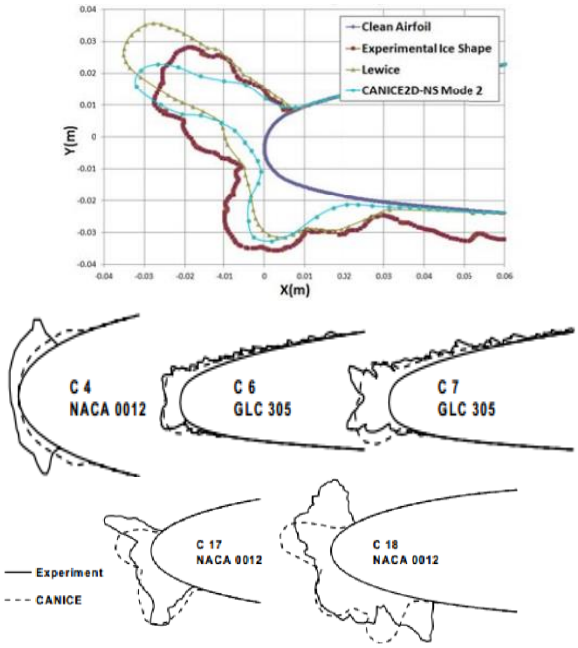

Figure 9: Prediction of ice shape under glaze conditions

4.2 Expansion of LEWICE Framework

The LEWICE icing software has been modified to include externally computed parameters. A schematic of the expanded simulation approach is provided in Figure 10. It depicts the

basic structure of how the airflow, droplet flow, and ice accretion modules interact. Although ice accretion is an unsteady phenomenon, this technique employs a quasi-steady approach is used to simulate ice growth. The quasi-steady assumption indicates that the impact of ice growth on both the flow and droplet fields is neglected during prescribed time intervals. This assumption is sufficient since the time scales between ice growth and aerodynamic changes are very different. Ice accretion occurs over a matter of minutes while aerodynamic fluctuations can occur in milliseconds.

Starting with grid generation, the process starts with creating the mesh and using the CFD software GENCAS to perform a flow analysis over a clean baseline configuration. The flow field information is then passed into the droplet trajectory module. The purpose of this module is to determine the local collection efficiency at surface. This parameter can be computed two ways. One technique uses the computed flow field from CFD simulations and calculates the droplet trajectory using the Lagrangian method available within the LEWICE software. The other uses an independent Eulerian based droplet solver, GTDROP. For the application of this study, the Eulerian trajectory analysis was chosen for increased accuracy. GTDROP reads the flow field data from GENCAS and computes the local collection efficiency (β) on the surface using the Eulerian method. This is then used as an input for LEWICE.

After the calculation of collection efficiency (internally or externally), LEWICE version 3.2.2 predicts the resulting ice growth along the surface for a set period of time. If ice accretion occurs over a long period of time or the produced ice shape is irregular and/or is very thick, a multi-shot approach is used. The multi-shot method reduces the time scaling between aerodynamic changes and ice accretion. In other words, the final ice shape is produced by including more frequent flow field updates and building up ice growth over shorter periods of time.

Utilizing the multi-shot technique transitions the process illustrated in Figure 10 to an iterative model. After the completion of ice prediction at each time step, the grid is

regenerated with the new iced airfoil geometry. Subsequent computations of the flow field and droplet trajectories will include the change in blade surface shape. The ice prediction analysis will then add new ice growth on top of the previous ice shape and the process is repeated until the total ice accretion time is reached.

This process is more appropriate for glaze or mixed ice shapes. Rime ice conditions can usually to be executed in a single-shot due to the small changes the ice shape adds to the original surface.

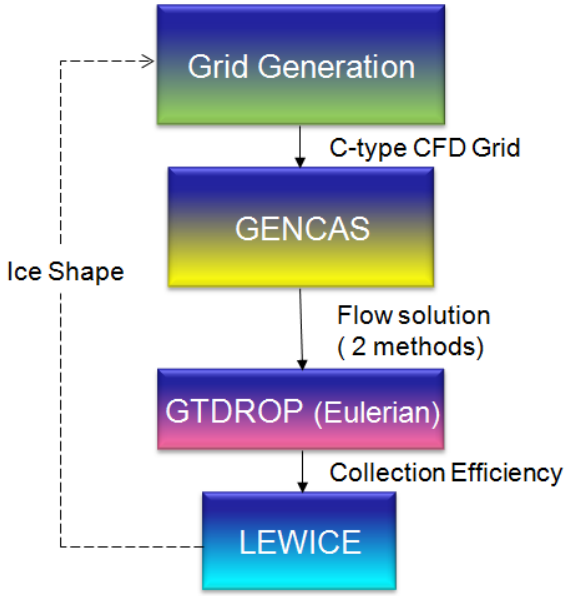

Figure 10: Modified LEWICE framework for 2-D ice accretion

4.2.1 Grid Generation: GTHybrid Gridgen

The first step in the quasi-steady analysis is to generate a C-type CFD mesh. There are several tools available but based on the researcher's prior experience, the GT Hybrid Grid Generator code was used to build the mesh. A grid with 300 grid points in the wrap direction and 10^{-6} chord normal spacing was produced for the two validation cases discussed at the end of this chapter. A far-field boundary of 10 chord lengths was also defined for the mesh. Figure 11 illustrates the grid used for the clean NACA0012 airfoil.

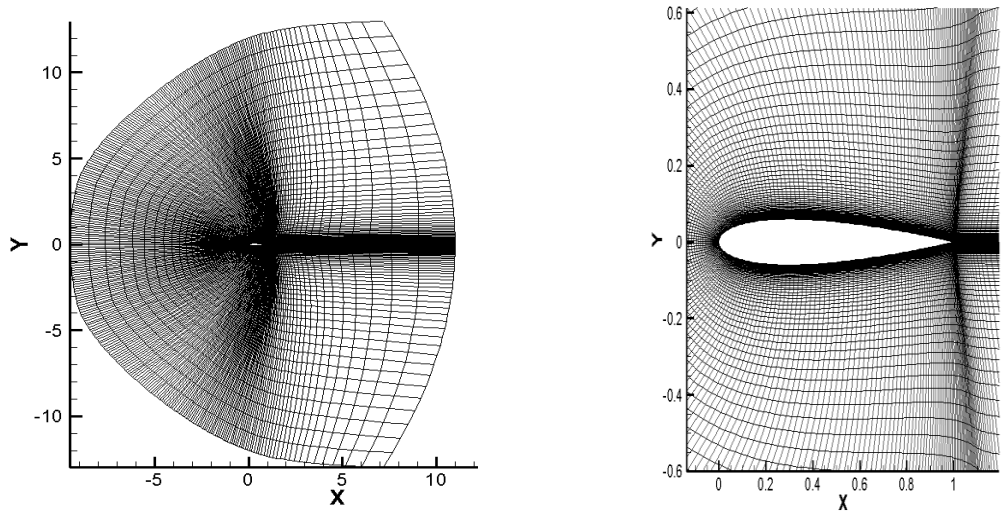

Figure 11: 300x121 grid for NACA0012

4.2.3 Flow field Analysis: GENCAS

A CFD code named GENCAS (Generic Numerical Compressible Airflow Solver), developed by Min is used in this study to model the flow field. GENCAS is a 2D/3D, structured multi-block, compressible and Euler/N-S CFD code [33] [34]. For the present validation cases, Roe scheme with 3rd order MUSCL reconstruction is used for flux calculations. A first order implicit LU-SGS scheme is used for marching in time. According to Nucci et. al., turbulence model in the CFD simulations has negligible effect on the predicted ice shapes at moderate angles of attack and subsonic Mach numbers [35]. Consequently, a fully turbulent boundary layer was assumed. This assumption may not be sufficient if future work requires heat transfer rates or skin friction coefficient obtain from CFD results are fed into LEWICE3.2.2.

4.2.3 Droplet Trajectory Analysis: GTDROP

GTDROP is an Eulerian based droplet solver used to compute the average water droplet properties within a control volume. The model solves the conservation equations of mass and momentum to obtain droplet flow field properties on the same mesh used in the CFD simulations. This physical approach has several advantages over the Lagrangian

approach which requires the tracking of individual water particles. Studies have shown an Eulerian method improves solution quality, has the ability to model unsteady flows over bodies in relative motion, and does automated treatment of shadow zones (no impingement) for probes or detector placing [36]. Also, the Eulerian approach is found to be more efficient because the Lagrangian approach requires a significant amount of seeding for accurate estimates of collection efficiency [37].

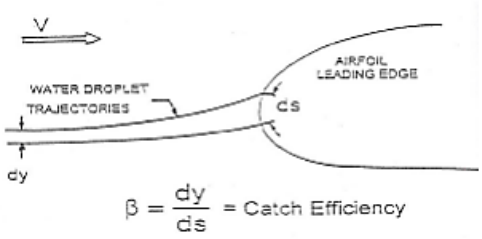

Figure 12: Graphic explaining how the collection efficiency (β) is calculated

GTDROP is specifically used to compute the local collection efficiency (β) along the wall the surface. Collection efficiency represents a common way of comparing droplet impingement rates at various flight conditions. It characterizes the configuration's ability to capture incoming water, seen in Figure 12. β is defined as the local mass flux of water on the airfoil surface normalized by the free stream liquid water content (LWC), and the frees tream velocity. In the equation below, α is the non-dimensional volume fraction of water, u_i is the non-dimensional velocity of droplets, ρ_w is the density of water, and A_i is the local area normal.

$$\beta = \frac{\alpha \rho_w u_i}{(LWC) U_\infty} \frac{A_i}{|A|}$$

4.2.4 Ice Prediction: LEWICE3.2.2

As a description of LEWICE was provided earlier, this section serves to describe the specific implementation of LEWICE. To determine the ice accretion, LEWICE requires the discrete body coordinates of the reference shape and an array of atmospheric and meteorological parameters as inputs. The atmospheric parameters include the air's static

temperature, pressure, density, and velocity. The meteorological parameters define the LWC, droplet diameter, relative humidity, and total time of icing exposure.

This research effort uses LEWICE version 3.2.2. The software program code consists of four major modules. They are 1) the flow field calculation, 2) the particle trajectory and impingement calculation, 3) the thermodynamic and ice growth calculation, and 4) the modification of the current geometry by addition the ice growth to it [28]. LEWICE3.2.2 offers several options which will modify or skip the calculation of certain parameters within each module. For the purposes of this study, the ability to bypass the potential flow and water trajectory solver was used. By initiating the appropriate flags, IBETA and ICP, LEWICE3.2.2 will read in supplemental input files which contain externally determined coefficient of pressure and the local collection efficiency along the body. The switch from potential flow solutions to CFD Navier-Stokes solutions and Lagragian particle tracking to Eulerian increases the ice accretion fidelity.

After bypassing the appropriate subroutines, the thermodynamic module will calculate the ice growth rate on each surface. With the specified time increment, the growth rate will be interpreted as an ice thickness and the body coordinates are recalculated to account for the accreted ice. The computational solver is exited at the completion of writing out the new geometry of the iced shape.

4.3 Validation Cases

The process for validation an icing code is challenging and consists of several steps, one of which is the comparison of code results to some known solution whether experimental or analytical. To validate the LEWICE icing code for 2D simulations, LEWICE results were compared against selected rime ice cases in a NACA0012 icing experiment tested in NASA Icing Research Tunnel (IRT) performed by Britton and Bond. A $1/6^{th}$ scale fuselage model of a UH-60A Black Hawk helicopter with a generic rotor was subjected to a wide range of icing conditions. The rotor blades had a diameter of 1.83 m (6 ft), a chord length

of 0.124 m (4.9 in), NACA0012 airfoil cross section, -10° of linear twist, and no chord tapering [38].

Since a helicopter in forward flight experiences changes in lift as it rotates from the advancing side to the retreating side, the local angle of attack is not a constant value. This creates a problem when attempting to model this situation within the steady state code LEWICE. In 1983, Korkan, Dadone, and Shaw developed a technique which simplified analysis of a helicopter's main rotor in forward flight with a rime ice accretion [39]. It was concluded that if the local Mach number and angle of attack produced by a helicopter performance code were averaged azimuthally, the predicted change in performance due to rime ice accretion differed by only ±2% over that of the traditional method of calculating values at specified azimuth locations around the disk. A similar averaging technique was used to create the LEWICE inputs. The local angle of attack at the radial location of interest is averaged azimuthally and the local velocity is the rotational velocity at the specified radial location. Two cases were chosen from this test, runs 34 and 41. The averaged velocity, angle of attack, and other icing environment variables are listed in Table 1.

The two runs were also repeated at the Vertical Lift Center of Excellence at the Pennsylvania State University on the recently developed the Adverse Environment Rotor Test Stand (AERTS) [40]. Results of this test are documented by a dashed red line, while the IRT's results are illustrated by a dashed blue line in the subsequent plots. Both LEWICE approaches are also plotted for comparison.

In the ice shape graphs, "Langragian Lewice" indicates potential flow calculation with Lagrangian droplet analysis and "Eulerian Lewice" refers to using CFD solutions and Eulerian droplet analysis for ice accretion.

Table 1: IRT Model Rotor Icing Test Conditions

Run	ΩR m/s	r/R	Temp °C	LWC g/m^3	MVD μm	AOA Deg.	Time sec
34	212.8	.45	-15.3	0.5	15	3.7	44
41	205.7	.4	-15.8	0.5	15	3.5	70

4.3.1 Run 34

The results of Run 34 represent rime ice accretion at the 45% radial span location. Icing was simulated for a total of 44 seconds. The atmospheric conditions are listed in Table 1. Although the ice accretion time is short, a multi-shot process was used. The ice accretion time was broken into two 22 seconds time segments.

Figure 13 shows the comparison of the simulated ice shape to the two icing tunnel experiments at the NASA Glenn IRT and Penn State's AERTS. Results from both LEWICE modes show reasonable agreement with the experimental data sets. The Eulerian method slightly over predicted the ice accretion on the upper surface. By investigating the collect efficiency, given in Figure 14, Eulerian droplet trajectory analysis has a slightly higher maximum collection efficiency shifted farther down the upper surface than the Lagrangian prediction.

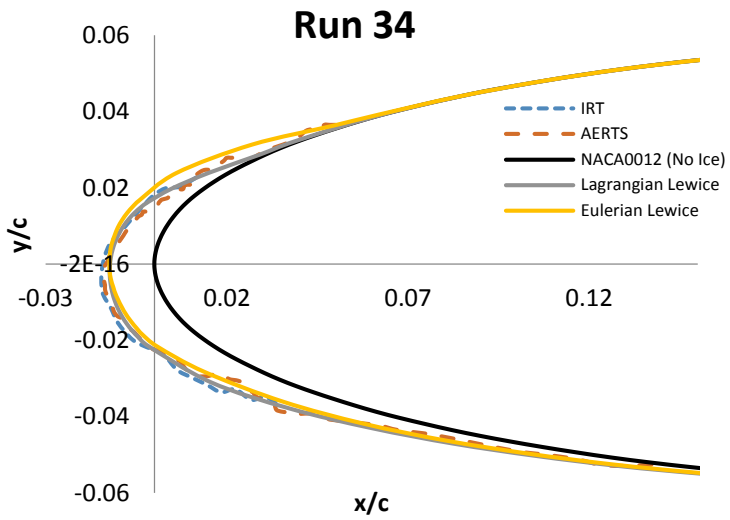

Figure 13: Ice shape of 44 sec rime ice accretion on NACA0012 airfoil at 45% R

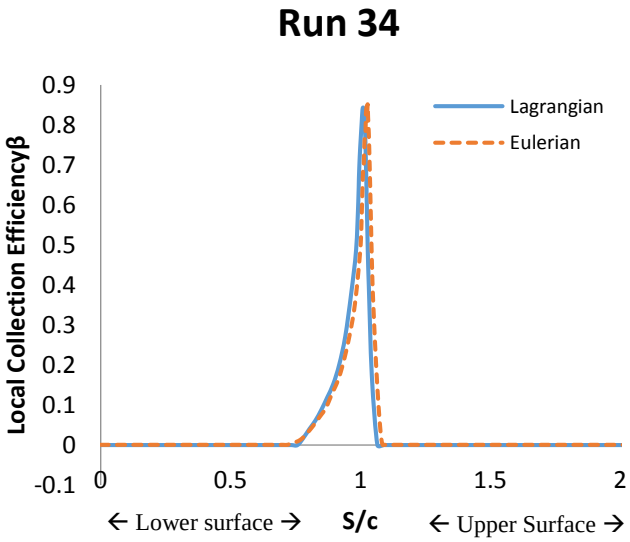

Figure 14: Comparison of Lagrangian solution and Eulerian solution for local collection efficiency

4.3.2 Run 41

Ice accretion simulation was completed for Run 41. The specified atmospheric conditions (listed in Table 1) instigated the formation of rime ice at 40% of the radial span. Ice accretion was simulated for a total time of 1.2 minutes. Figure 15 shows the comparison of the simulated ice shape to the two icing tunnel experiments at the NASA Glenn IRT and Penn State's AERTS. Both LEWICE methods show a reasonable prediction of the ice

shape. Small discrepancies can be seen at the leading edge and the overall roughness of the ice shape. The Eulerian droplet trajectory analysis generated an ice shape that more closely matches experimental data. Figure 16 illustrates the collection efficiency results between the two methods. The solutions are very similar but Eulerian predicted collection efficiency is shifted farther down the upper surface. This accounts for the over predicted ice accretion along the upper surface.

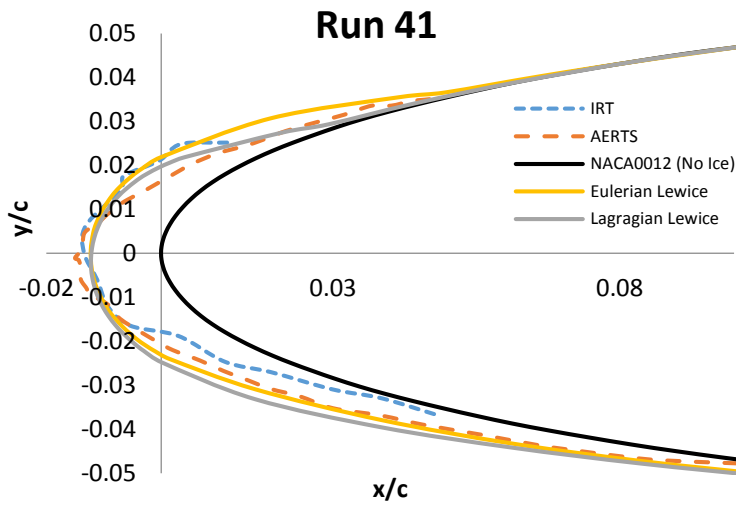

Figure 15: Ice shape 70 sec rime ice accretion on NACA0012 airfoil at 40% R

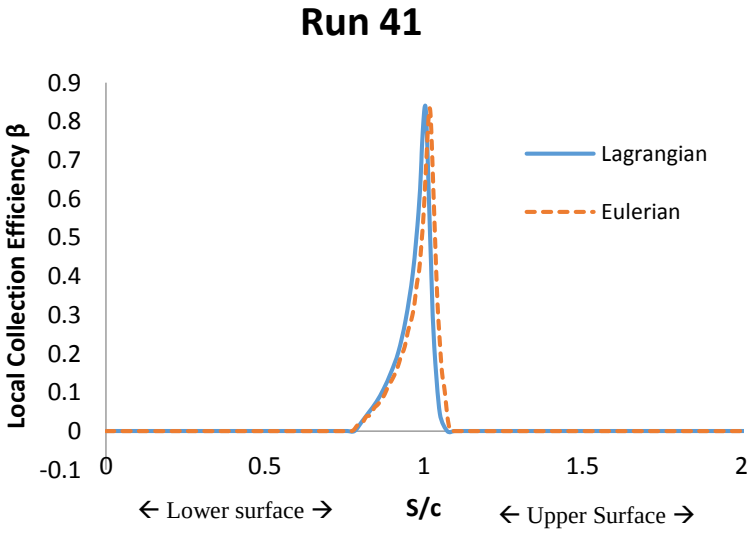

Figure 16: Comparison of Lagrangian solution and Eulerian solution for local collection efficiency

CHAPTER 5

INCORPORATION OF SPANWISE FLOW INTO NUMERICAL SIMULATIONS

This chapter serves to describe the final aim of this work, creating a pseudo three dimensional ice accretion solver by modifying the two dimensional LEWICE program to incorporate the influence of span-wise flow experienced by rotor blades.

The chapter begins by overviewing of the problem at hand and discussing the required actions to complete the objective. The next section outlines the architecture of the methodology. This research effort stems from the 2-D methodology described in Section 4.2, but incorporates several modifications for analyzing a three dimensional blade. As previously mentioned, simulating ice growth requires coupling of different physical models. The new programs utilized are (1) Chimera Grid Tools, a grid generator, (2) GT-Hybrid, a Navier-Stokes CFD solver, (3) Tecplot, a graphical tool used for streamline integration, and (4) multiple scripts for final ice shape interpolation. The background of each tool are described along with a discussion of its application within the study's architecture. A brief description of the automation process is also provided.

The final sections discuss the results of two test conditions when the influence of span-wise flow is incorporated within LEWICE. The generated ice shapes are compared to the traditional strip theory method and assessed.

5.1 Research Focus and Objectives

Numerical solvers increase in complexity when a third dimension is added to the analysis. A reduction in computational time can be achieved by splitting a three dimensional shape

into a series of two dimensional cutouts. Computational solutions are acquired at each cutout individually, and then integrated over surface to produce the final three dimensional solution. This methodology, known as "strip theory", is typically used to generate ice growth along a wing or rotor blade. Using strip theory forces the assumption that ice only grows along constant $\frac{r}{R}$ or $\frac{y}{b}$ lines (illustrated in Figure 17). However, swept wings and rotor blades experience significant span-wise flow from flow separation or, in the case of rotor blades, centrifugal forces.

To emphasize of the scale of span-wise influence on rotor blades, an image of the oil flow lines on a rectangular wing is provided in Figure 18, followed by an illustration of the surface streamlines for a rotor blade traversing through one revolution (Figure 19). The oil flow patterns in Figure 18 denote a lack of span-wise flow since oil lines are perpendicular to the horizontal leading edge. In comparison, the rotor blade's curved flow path is very apparent at each azimuthal angle.

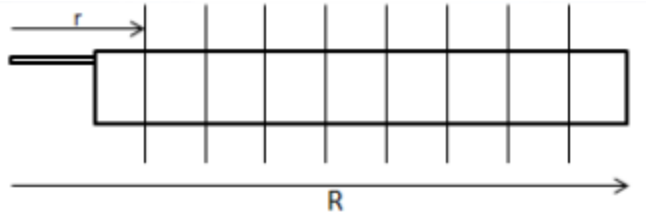

Figure 17: Illustration of a blade divided into a series of 2-D cutouts with strip theory

Thus, it may be more appropriate to calculate ice accretion in the direction of the actual flow path, i.e. a body's surface streamlines. The migration of water droplets along the surface streamlines may cause ice to grow in an entirely different manner creating a larger build-up of ice at the wing or blade tip. Also, when the leading edge is heated, the runback of the water droplets are not likely to follow the $\frac{r}{R}$ constant lines, but along the streamlines and could refreeze at unfavorable locations. This phenomenon has not been adequately explored. Thus, goal of this research is to examine how the influence of span-wise flow over rotor blades affect ice accretion.

The following activities are required to evaluate the change in ice accretion behavior due to span-wise flow

- Computation of the flow field over a three dimensional rotor blade
- Visualization of the surface streamlines
- Calculation of the local collection efficiency and coefficient of pressure along the surface streamlines
- Analysis of ice accretion over three dimensional rotors blades using the classical LEWICE strip theory method
- Analysis of ice accretion using the calculated streamline collection efficiency and pressure coefficient data
- Comparison of both method's resulting ice shapes at several radial stations along the blade span at azimuthal locations: $\Psi = 0°$, 90°, 180° and 270°

Figure 18: Flow visualization for a straight wing aircraft [41]

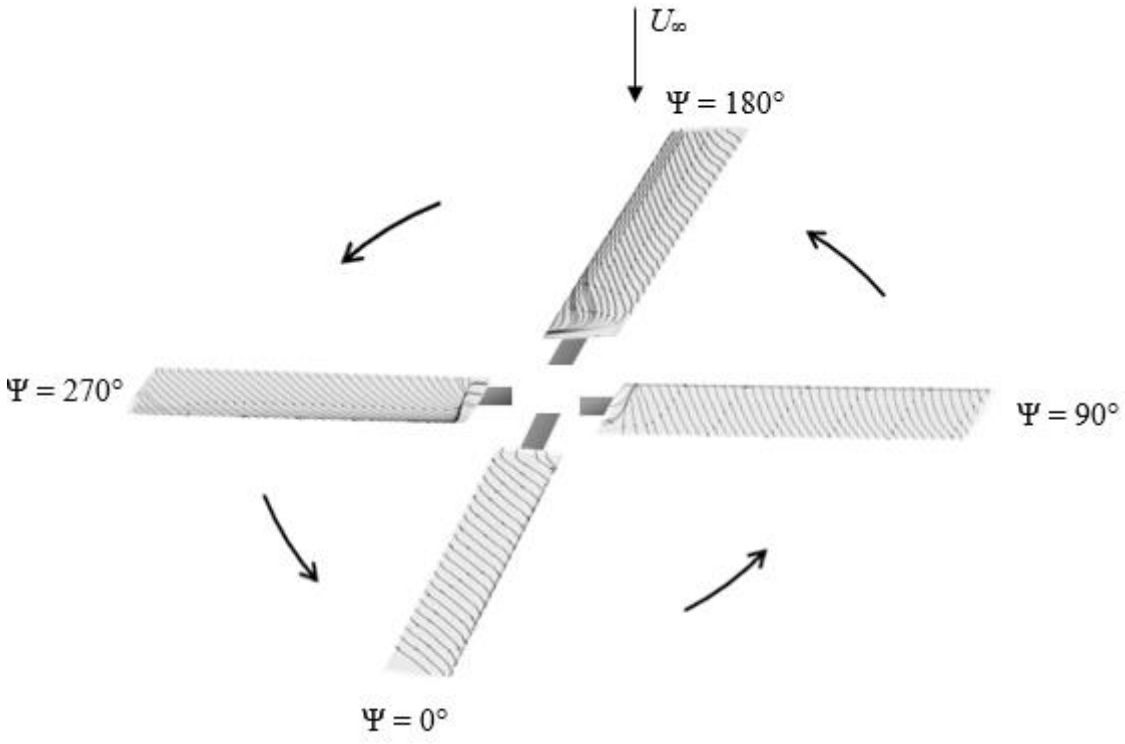

Figure 19: Surface streamlines of a rotor blade traversing around the disk of revolution.

5.2 Procedure Modifications

A schematic of the simulation approach use for ice prediction of three dimensional rotor blades is provided in Figure 20. It depicts the basic structure of how the different modules required for ice accretion simulation interact with one another. Depending on the user

input, the functional architecture has the ability to switch between an iterative or non-iterative system. The procedure is very similarly to the methodology for two dimensional airfoils, but requires additional steps and different tools to produce the final ice shape.

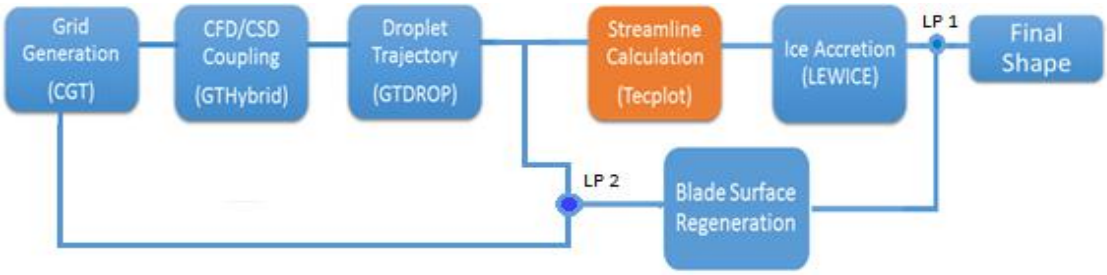

Figure 20: Overview of the ice accretion methodology incorporating the additional streamline calculation step

The process starts with the grid generation of a C-H mesh using a set of scripts provided in NASA's Chimera Grid Tools. The output of this step is a required input for subsequent modules in the methodology.

Next, a flow analysis over a clean baseline configuration is performed. Unlike in the methodology in the previous chapter, the flow field is determined through a coupled CFD/CSD simulation. Here, the CSD analysis is completed using a harmonic blade balancing script and computes the necessary blade flapping angles for the CFD solver GTHybrid. This step is followed by the prediction of droplet trajectories. The local collection efficiency at surface is determined using the Eulerian method.

The completion of flow field and trajectory calculations brings the procedure to the span-wise modification step. Streamline locations are integrated along the surface using the graphical tool Tecplot360. The corresponding coefficient of pressure (c_p) and collection efficiency (β) data are then extracted and processed into LEWICE input files. Ice is then grown at every radial station across the blade using LEWICE3.2.2.

The procedure now passes through a logic point represented in the illustration as "LP 1". Here, the number of azimuth iterations is determined. If ice accretion at more than one azimuth station is desired, the process will transform into a multi-shot approach.

If icing occurs over a long period of time or the produced ice shape is irregular and/or is very thick, a multi-shot approach is used. This triggers the logic point, "LP 1" in the procedure. The multi-shot iterations are similar to the process used for two dimension shapes. As before, the time step is segmented into a shorter periods of time. For rotor blades, the new time step, T_{seg}, is found by dividing the total accretion time by the total number of revolutions, N_{rev}, multiplied by the number of azimuthal stations , N_{Ψ} for Typically, the disk is divided into four azimuth stations at 0°, 90°, 180°, and 270°.

$$T_{seg} = \frac{T_{total}}{N_{rev} * N_{\psi}}$$

However, there are now two different ways to complete a multi-shot approach. This functionality is illustrated by the feedback loops at logic point 2, "LP 2". The top feedback loop indicates that the flow field and droplet trajectories are not recalculated at each time step. This method is appropriate when the icing time is under 4 or 5 minutes and the ice shapes are nominal. If the new shape is significantly different, the procedure chooses the bottom feedback loop. Now, the iced blade surface must be fully re-gridded in order to recalculate the rotor flow field and droplet trajectory.

After determining the streamline data, LEWICE will now accrete ice on top of the previous ice shape. The process repeats itself until the total ice accretion time is reached. Rime ice conditions can usually be executed in a single-shot due to the small changes the ice shape adds to the original surface.

5.2.1 Grid Generation: Chimera Grid Tools

The first step in the quasi-steady analysis is to generate a C-H type grid. There are several tools available to accomplish this, but based on the researcher's previous experience, Chimera Grid Tools (CGT) was used. CGT is a package consisting of numerous gridding tools created by NASA Ames Research Center [42]. CGT's HYPGEN program was used to generate a three dimensional volume grid over a blade surface grid. HYGEN generates the grid by marching from the initial surface using hyperbolic methods.

The present study incorporates a 131 x 90 x 45 grid with 10^{-4} chord normal spacing illustrated below in Figure 21. A far-field boundary of 9 chord lengths was also defined for the mesh. Figure 22 illustrates an enlarged image of the blade's airfoil shape. The airfoil consisted of a NACA0012 airfoil with an additional heater blanket wrapped around the leading edge.

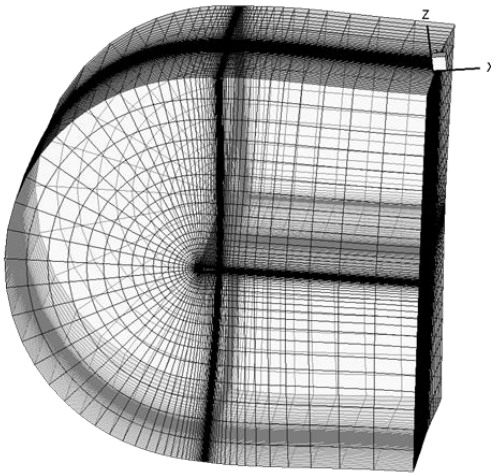

Figure 21:131x90x45 C-H mesh produced using CGT

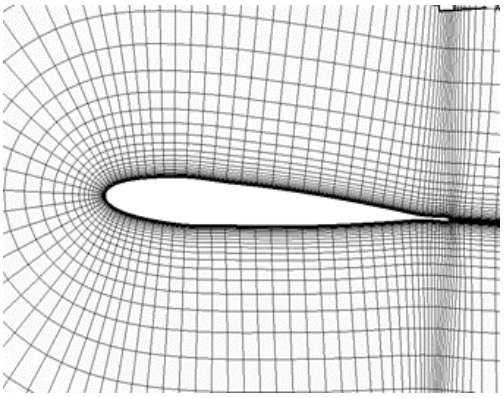

Figure 22: The NACA0012 airfoil modified with an additional heater blanket at the leading edge

5.2.2 CFD/CSD Solver: GTHybrid with Harmonic Balancing script

The computation of the rotor's flow field was completed using GTHybrid. GTHybrid is a three-dimensional, unsteady, viscous, compressible flow solver that uses a free wake solver to model the effects of the rotor wake. The flow is modeled from first principles using the Navier-Stokes methodology. The Navier-Stokes equations are integrated in time by means of an approximate LU-implicit time marching scheme. SA-DES turbulence model is used to compute the eddy viscosity. For this application, the flow was assumed to be turbulent everywhere, and hence no transition model was incorporated [43].

In this study, results were generated using a Bell 206 tail rotor system consisting of a rigid 2 blade teetering rotor with a δ_3 of 45°. Although the assumption of a rigid blade removes the complexity of aerodynamic and structural dynamic coupling from blade

deformations, the hinge offset will. The $\delta_3 = 45°$ creates a system with pitch-flap coupling. As a blade flaps up, the δ_3 offset pitches the blade nose up, resulting in an increase in thrust. Unlike other CFD solvers, GTHybrid does not internally compute the blade motions as it travels around the disk of rotation. In order for the CFD simulation to accurate predict the rotor airloads, this research effort incorporated a loosely coupled harmonic balancing approach.

The iterative harmonic balancing approach, informally formulated by Dr. Ritu Marpu and Jeewoong Kim, is a method which estimates the flapping angles after every coupled CFD iteration until the hub roll and pitching moments are removed. The process is represented by the following steps

1. **A classical linear aerodynamics calculation is performed.** From those results, initial flapping angles β_0, β_{1c} and β_{1s} are estimated. These estimated angles are used to create a blade motion file, a required input for GTHybrid. For a teetering rotor with no coning $\beta_0 = 0$.
2. **A CFD analysis is then computed.** The first iteration of this process is denoted as Iteration-0. The sectional lift, L'_{CFD}, as function of azimuth and radial location is obtained. Typically CFD solvers normally save C_nM^2. Thus,

$$L'_{CFD} = \frac{1}{2}\rho\, c\, a_\infty^2\, C_n M^2$$

3. **The pitching and rolling moments at the hub are calculated using the CFD data.** If the flapping angles are exact, the hub moments are equal to zero.
4. **Values of $\Delta\beta_{1c}$ and $\Delta\beta_{1s}$ are calculated in order to account for any imbalance in the rolling and pitching moments at the hub.** Since the flapping dynamics are based on simplified linear aerodynamics in Iteration-0, the hub moments (or the sine and cosine components) will not go to zero. Essentially, the azimuthally averaged M_{roll} and M_{pitch} at the hub are functions of β_{1c} and β_{1s}. A flapping angle

correction, $\Delta\beta_f$, must be added to the current best estimates in order for M_{roll} and M_{pitch} to equal zero.

$$M_{roll}(\beta_{1c},\beta_{1s}) = M_{roll}\left(\beta_{1c}^{current\_guess} + \Delta\beta_f, \beta_{1c}^{current\_guess} + \Delta\beta_f\right) = 0$$
$$M_{pitch}(\beta_{1c},\beta_{1s}) = M_{pitch}\left(\beta_{1c}^{current\_guess} + \Delta\beta_f, \beta_{1c}^{current\_guess} + \Delta\beta_f\right) = 0$$

By expanding the above two equations about the current guess for β_{1c} and β_{1s} and inverting the subsequence matrix (shown below) finds $\Delta\beta_{1c}$ and $\Delta\beta_{1s}$.

$$\begin{bmatrix} \frac{\partial M_{roll}}{\partial \beta_{1c}} & \frac{\partial M_{roll}}{\partial \beta_{1s}} \\ \frac{\partial M_{pitch}}{\partial \beta_{1c}} & \frac{\partial M_{Pitchl}}{\partial \beta_{1s}} \end{bmatrix} \begin{Bmatrix} \Delta\beta_{1c} \\ \Delta\beta_{1s} \end{Bmatrix} = -\begin{Bmatrix} M_{roll} \\ M_{pitch} \end{Bmatrix}_{CFD}$$

5. **The $\Delta\beta_{1c}$ and $\Delta\beta_{1s}$ quantities are added to the most recent estimates of β_{1c} and β_{1s}**
6. **Steps 3-5 are repeated until the hub roll and pitching moments all go to zero.**

Typically, the process is repeated three times before the hub moments converge to zero. Once convergence is reached, hub loads, flow field, and grid information are passed to the remaining ice analysis modules using standard PLOT3D format.

5.2.3 Streamline Integration: Tecplot360

After running GTDROP to find the local collection efficiency, the next step defines the streamline locations along the rotor blade surface. Tecplot360, a commercial CFD visualization tool, was used to locate the streamlines. As mentioned in a previously, streamlines are used to illustrate the nature of the vector field flow. When placed on a no-slip boundary surface, streamlines propagate according to the normal gradient of the tangential velocity (proportional to shear stress) near the surface. Calculation of streamlines in Tecplot use a two-step second-order Runge-Kutta method described below [44].

1. The velocity vector direction is calculated at the current particle position.
2. A small step is made and the velocity vector direction is calculated at the new location.
3. The vectors obtained in 1 & 2 are averaged and the resulting vector is re-applied at the initial position. The weights of this averaging enforce formal second-order accuracy. Velocities at each point are calculated using tri-linear interpolation.

From a data array containing the U, V, and W velocity components, blade surface grid geometry, and surface c_p and β, a series of upper and lower surface streamlines are created at every radial station defined by the CGT grid. Figure 23 illustrates a rotor blade with upper and lower surface streamlines at every radial index. A single streamline is provided just for visual clarity.

In order to create both upper and lower streamlines that start from the same radial index of the blade, each streamline path must be defined to intersect the chord-wise index closest to the leading edge stagnation point. All streamlines are extracted to a Tecplot formatted file which contains the corresponding x, y, z, c_p, and β values.

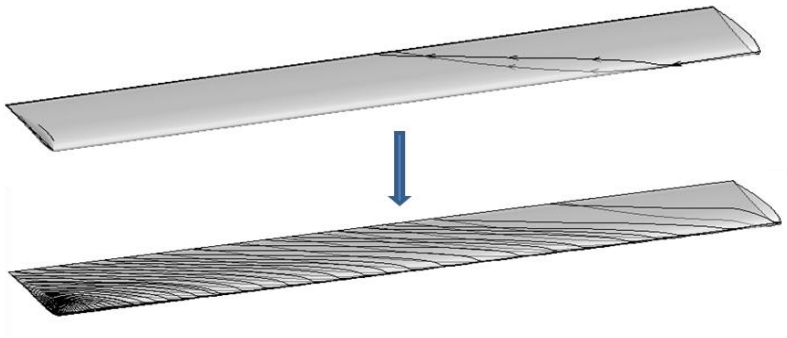

Figure 23: Streamlines created in Tecplot360 at every radial station for a total of 51 streamlines. A single streamline is provided for a simplified illustration

By directing each streamline to specifically pass through the location closest to the leading edge stagnation point, several issues arise that must be corrected. First, the

technique tends to fail in regions near the blade root and tip. When the rotor blade traverses through the retreating side, regions of separated flow are likely to occur at the blade root. Detached flow cannot be modeled as streamlines and thus, will not capture the necessary data points. In addition, flow at the tip is highly influenced by span-wise flow. When forcing the streamlines to pass near the stagnation point, the projected flow trajectories sweep quickly off the blade edge. This creates extremely short streamlines that do not contain enough data points for LEWICE. An example of the blade tip streamlines are illustrated in Figure 24. For these two areas, flow field, collection efficiency, and geometric information must instead be extracted along the corresponding r/R perpendicular cutouts.

Figure 24: Zoomed in image of the blade tip streamlines

Next, all pathlines originate from the leading edge of the blade root. Figure 25a illustrates this characteristic with the referenced area circled in red. Data points within the circled region are considered unnecessary and must be removed from the data array. Only streamline locations with y values that greater than or equal to the desired radial station are kept.

The last modification pertains to the gap in values produced at the leading edge, as seen in Figure 25b. In order to create separate lower and upper surface streamlines, paths were directed to intersect the closest chord-wise index before and after the stagnation point, respectively. The missing values were filled by using data from the r/R perpendicular cutout and inserting it into the streamline file.

An example of a corrected streamline is provided in Figure 26. Once modifications are complete, the streamline data is reconstructed to fit the formatting required LEWICE input files rflow.inp, containing the surface pressure coefficient values, and rbeta.inp, surface collection efficiency values.

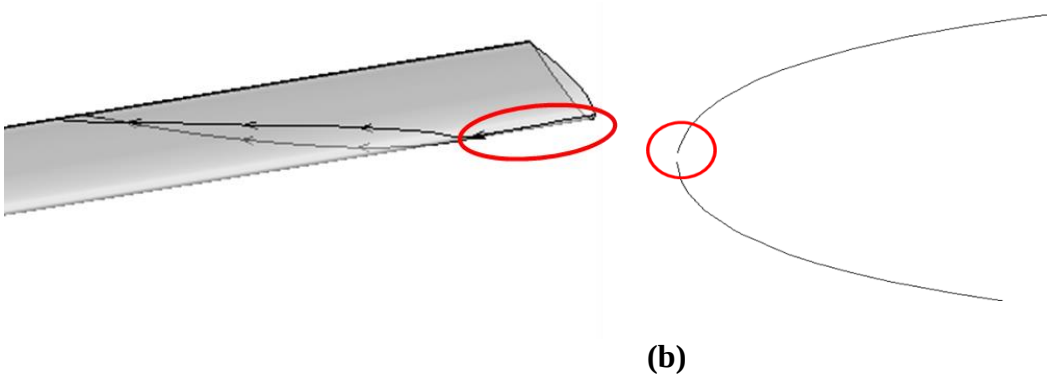

(a) **(b)**

Figure 25: Streamline areas, circled in red, that require data manipulation to recreate values into LEWICE friendly input files: (a) extraneous values contained within each streamline, (b) gaps located at the leading edge when viewed on the x-z plane

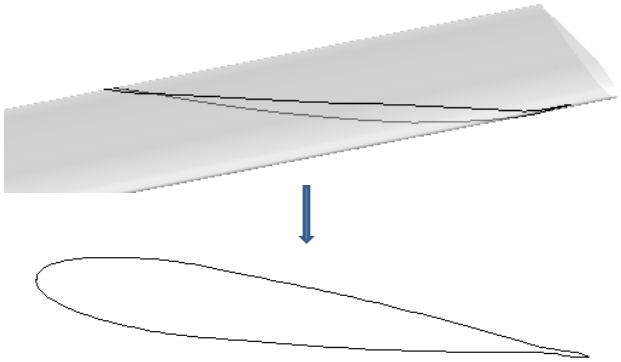

Figure 26: Modified streamline projected onto the two dimensional x-z plane

5.2.4 Streamline Ice Shape Interpolation

Once the ice has been predicted using LEWICE, further post processing is required to find the actual ice shape. This additional step is required since the ice predictions were calculated using the streamline c_p and β values, but are replaced back into the blade geometry along the constant r/R perpendicular cutout (see Section 5.3 for more details).

Finding the final shape of the predicted ice on the streamline's coordinates requires interpolation. This purpose of this section is to explain each step involved in the interpolation methodology.

Determination of Ice Thickness and Orientation Angle

The first step in this process is the determination of the ice thickness and the orientation angle. This is completed by comparing the body coordinates of the new iced shape, (x^n, z^n), to the previous body shape, (x^{n-1}, z^{n-1}), at each chord-wise index, "*i*", along a constant radial location, "*j*". The ice thickness, *t*, is defined as the distance between the two points. The orientation angle, θ, is the angle offset between the new body coordinates and the pervious shape. A graphical representation of these two parameters is provided in Figure 27.

$$t_{i,j} = \sqrt{\left(x_{i,j}^{n} - x_{i,j}^{n-1}\right)^2 + \left(z_{i,j}^{n} - z_{i,j}^{n-1}\right)^2}$$

$$\theta_{i,j} = \tan^{-1}\left(\frac{z_{i,j}^{n} - z_{i,j}^{n-1}}{x_{i,j}^{n} - x_{i,j}^{n-1}}\right)$$

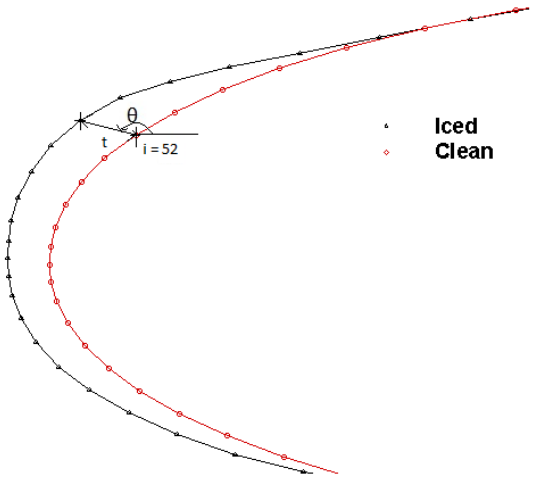

Figure 27: Example of the ice thickness, t, and angle of placement, θ, after the first iteration

The parameter θ is defined as positive in the counter clockwise direction. As such, it requires the following equations to enforce proper orientation. After iterating through the entire blade surface, an i_{max} x j_{max} matrix is created for *t* and θ.

$$\theta_{i,j} = \begin{cases} \theta_{i,j} + \pi, & z_{i,j}^{n} - z_{i,j}^{n-1} > 0;\ x_{i,j}^{n} - x_{i,j}^{n-1} < 0 \\ \pi, & z_{i,j}^{n} - z_{i,j}^{n-1} > 0;\ x_{i,j}^{n} - x_{i,j}^{n-1} = 0 \\ \theta_{i,j} + \pi, & z_{i,j}^{n} - z_{i,j}^{n-1} < 0;\ x_{i,j}^{n} - x_{i,j}^{n-1} < 0 \\ \theta_{i,j} + 2\pi, & z_{i,j}^{n} - z_{i,j}^{n-1} < 0;\ x_{i,j}^{n} - x_{i,j}^{n-1} > 0 \\ \frac{3\pi}{2}, & z_{i,j}^{n} - z_{i,j}^{n-1} < 0;\ x_{i,j}^{n} - x_{i,j}^{n-1} = 0 \\ 0, & t = 0 \end{cases}$$

Determination of Closest Blade Surface Point

Next, the blade surface body coordinate closest to the streamline point must be determined. Starting with the first streamline point, $S_{1,1}$, the distance relative to every blade surface point, P, is computed. The closest point is defined as the location with the minimum distance. This process is repeated until every streamline point has an associated minimum distance point P. Figure 28 is a representation of this procedure. In the illustration, the point closest to the streamline point $S_{90,1}$ would be defined as point $P_{50,3}$.

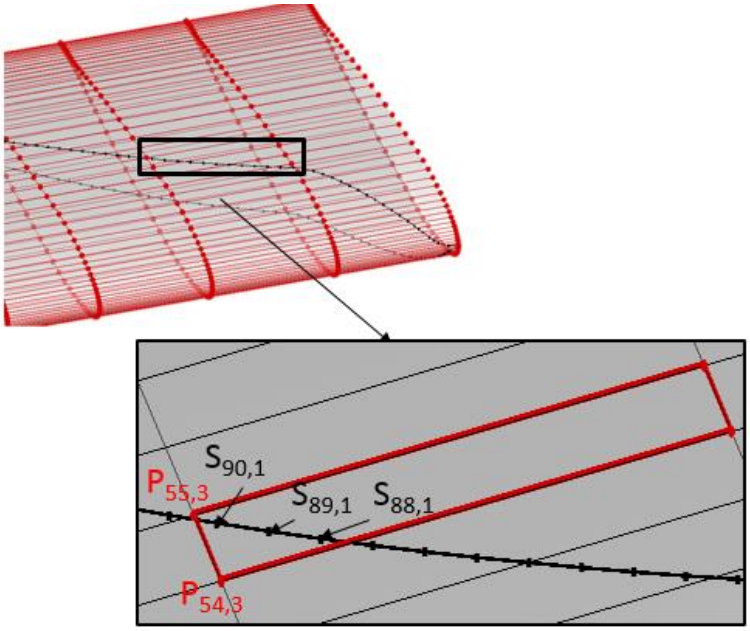

Figure 28: Illustration of closest blade surface geometry points (P) to streamline points (S)

Location of Most Influential Points

The interpolation process uses a weighting function which places greater shape influence from points closer to the streamline point of interest. Thus, each of the new streamline body coordinates are determined based off of the ice thickness and placement orientation details of only four points which surround the streamline point of interest. The box corners are chosen using the placement orientation of the closest point, found in the previous step, to the streamline point. In other words, the closest perpendicular cutout point "P" is the first known corner of the surrounding box. Determining the other corners of the box will rely on how point P lies in reference to the streamline point "S".

Using a FORTRAN script, Point P is denoted as either forward or backwards and to the left or to the right of the point S. From here, the script will appropriately index in the *i* and/or *j* direction and flag three other points as the corresponding box indices. The four points are denoted as P_1, P_2, P_3, and P_4.

For an example, Figure 29 is an illustrations of the box of points surrounding the streamline point $S_{90,1}$. Here, P_1, located at $i_{P_1} = 55$ and $j_{p_1} = 3$, is the closest perpendicular cutout point found in the previously step. Since the streamline runs along the upper surface, P_1 is forward and to the right of $S_{90,1}$. P_1 is considered forwards due to all *i* indices wrapping from the lower surface of the trailing edge, i =1, to the upper surface of the trailing edge, $i = i_{max}$. The next corner, P_2, is found by moving backwards from P_1 and along the same radial line, i.e. $i_{P_2} = i_{P_1} - 1$ and $j_{P_2} = j_{P_1}$. To the right is point P_3 at $i_{P_3} =$ and $j_{P_3} = j_{P_1} - 1$. Finally, P_4 is found at $i_{P_4} = i_{P_1} - 1$ and $j_{P_4} = j_{P_1} - 1$.

After defining the *i* and *j* indices of the four corners, the associated ice thickness and orientation angle are stored as the parameters t_i and θ_i.

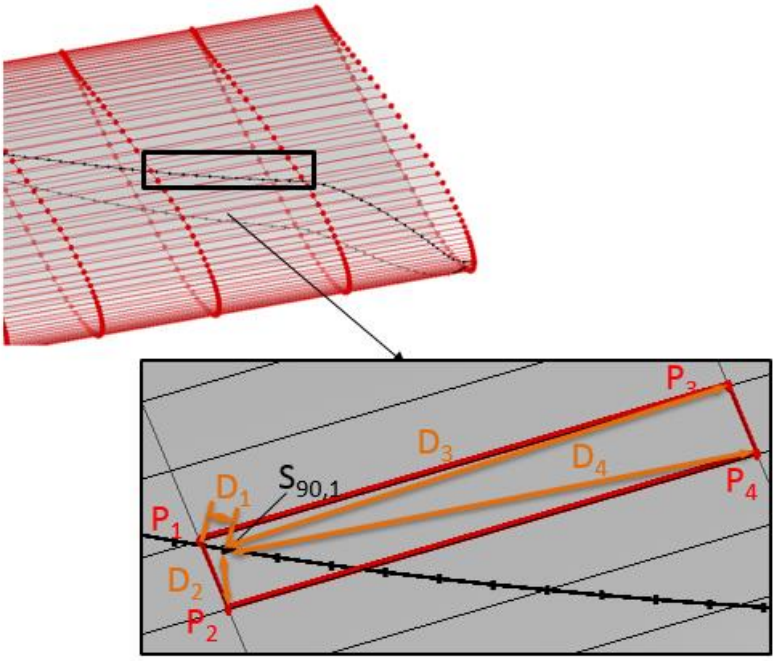

Figure 29: Box of four closest blade surface points (P_1-P_4) to the streamline point $S_{90,1}$. The corresponding distances between the four locations are denoted as D_1-D_4

Determination of new x and z body coordinate for streamline points

As previously mentioned, the interpolation process incorporates a weighting function based on the distance between the cutout geometry and the streamline point. The distance, D_i, is described by the following equation below. A constant parameter of $\varepsilon = 0.0001$ is added to ensure future calculations do not create indeterminate answers.

$$D_i = \sqrt{\left(x_{p_i} - x_s\right)^2 + \left(y_{p_i} - y_s\right)^2} + \varepsilon$$

Once the distance from the streamline point, $S(x_s, y_s)$, to the four corners of the box $P_i(x_{p_i}, y_{p_i})$ are known (see Figure 29 for a visual representation). The new streamline ice thickness and orientation angle are found.

$$t_{i,j} = \left(\frac{t_1}{D_1} + \frac{t_2}{D_2} + \frac{t_3}{D_3} + \frac{t_4}{D_4}\right) \div \left(\frac{1}{D_1} + \frac{1}{D_2} + \frac{1}{D_3} + \frac{1}{D_4}\right)$$

$$\theta_{i,j} = \left(\frac{\theta_1}{D_1} + \frac{\theta_2}{D_2} + \frac{\theta_3}{D_3} + \frac{\theta_4}{D_4}\right) \div \left(\frac{1}{D_1} + \frac{1}{D_2} + \frac{1}{D_3} + \frac{1}{D_4}\right)$$

Finally, the new iced streamline coordinates are computed using the following equation. x_s^n denotes the current iteration step while x_s^{n-1} represents the previous iteration.

$$x_s^n = x_s^{n-1} + t_s \cos\theta_s$$

$$z_s^n = z_s^{n-1} + t_s \sin\theta_s$$

The steps descried in this section are repeated until every streamline index has been recalculated.

5.2.5 Blade Surface Grid Regeneration

Techniques to recreate a structured mesh over the iced geometry's surface were not formulized within this thesis. Ideas for grid regeneration will later be discussed in the work's conclusion, Section 6.2.

5.3 Methodology Automation

The framework to find the ice accretion along surface streamlines is a labor intensive procedure, only partially automated using two python scripts. A breakdown of module automation is provided in Figure 30. The first script initiates the grid generation, CFD/CDS coupling, and droplet trajectory analysis. This portion of the procedure takes the longest computational time due to several iterations of CFD/CSD coupling. After the flow field and collection efficiency are computed the automation process stops and the user is required to generate the streamline locations in Tecplot.

Next, a second python script successively iterates across the blade's radial stations and predicts the ice accretion. Once the ice at a particular radial station is computed, the new shape is inserted back into the blade's surface grid. By the last radial location, i.e. the blade tip, the blade surface geometry will have been completely updated to include the additional ice thickness.

When the blade geometry is finalized the python script finishes and the process is continued through a series of individual programs and post processing scripts. These

additional steps, represented by the green dashed box in Figure 30, are used to interpolate of the resulting iced streamline geometries and recreate the blade surface grid.

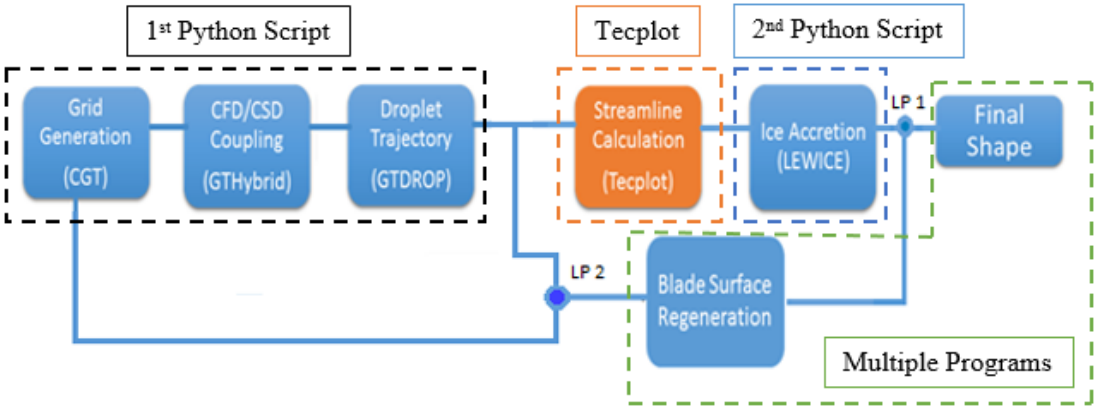

Figure 30: Illustration designating which modules are controlled by automated Python based scripts

5.4 Results and Discussion

This final section discusses the results of two test conditions that include the presence of span-wise flow. For the purposes of the research effort, only a single shot approach was used. The difference between the streamline ice shape and the normal strip theory prediction after one iteration is sufficient to examine the influence of span-wise flow. For the first test condition, ice accretion is computed at four different azimuth locations in order to assess how varying degrees of span-wise affect the results. The four chosen locations are 0°, 90°, 180°, and 270°. Refer to Figure 19 for nomenclature orientation. The second case was chosen to assess the effect of glaze icing conditions. Generated ice shapes are compared to the traditional strip theory method at multiple radial locations along the blade span.

5.4.1 Description of Model and Test Conditions

The new methodology is exercised on a set of conditions performed in an icing tunnel test conducted by the Vertical Lift Consortium. The project, entitled “High Fidelity Icing Analysis for Rotors”, completed extensive rotor blade ice testing in NASA Glenn’s

Icing Research Tunnel (IRT) in September 2013. The tested rotor system was a production Bell Helicopter Model 206B tail rotor blade with heater blankets bonded to the blade surface. The tail blade had an NACA0012 airfoil shape, a chord of 5.3", and a blade radius of 32.6". An image of the test model is provided in Figure 31.

This particular experiment was chosen due to the expansive set of icing conditions tested and the novel way the iced geometry was recorded. In prior experiments, results were documented by tracing the ice shape by hand. The VLC project utilized NASA's 3-D scanning capabilities to create scanned images of the blade. Figure 32 shows an example 3-D scan with a photograph of the same ice shape. At the time of this writing, the results of the icing experiment have not been publically released. However, any future additions to this work will have the ability to compare results to actual experimental data for validation purposes.

Figure 31: Model Bell 206 tail rotor used in an icing tunnel test at NASA Glenn Research Center's Icing Research Tunnel

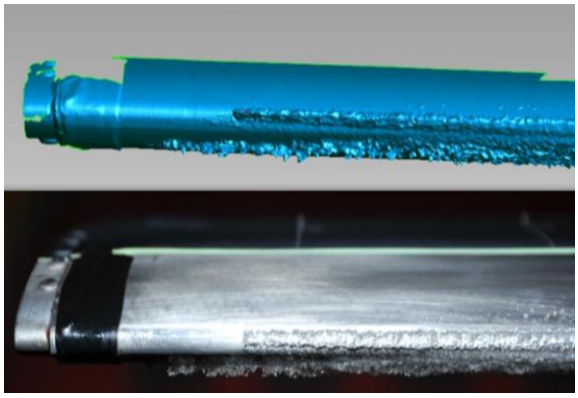

Figure 32: Example of a 3-D scan of rotor blade ice compared to the actual experimental ice shape

Two icing conditions were pulled from the experiment's test matrix with one additional dry test case for performance validation. Description of the test cases are provided in Table 2. In these simulations, the droplet diameter, LWC, airspeed, and advanced ratio remained consistent. For the purpose of this report, ice accretion time was decreased by a fourth of the total experimental icing time. Ice prediction results are given

in the Appendix of this work. At each azimuth, 2-D projections of the blade's streamlines are provided before the set of predicted ice shapes.

Table 2: Test case conditions from the VLC icing tunnel experiment

Case	Airspeed (kts)	RPM	Advanced Ratio	Temp °C	LWC g/m^3	MVD μm	Mast Tilt (deg)	Collective Pitch (deg)	Time (sec)
81	60	1200	.298	-10	---	---	-5	0, 2, 5, 8, 10	---
2	60	1200	.298	-30	0.5	15	-5	8	50
53	60	1200	.298	-10	0.5	15	-5	2	45

5.4.2 Clean Rotor Performance Validation

For flow field validation, the calculations produced from the CFD/CSD's method were compared to Case 81's performance characteristics. Case 81 represents a dry air test for a sweep of collective pitch angles 0°, 2°, 5°, 8°, and 10° with each angle sustained for around 20 seconds. The tunnel was run at an ambient temperature of -10° C (14° F) and 60 kts. For other parameters, refer to Table 2.

Thrust and power are compared after every iteration of the harmonic balancing method, respectively denoted as Itn-0 through Itn-2 on Figure 33 and Figure 34. Figure 33 illustrates the results of the CFD/CSD coupling at each collective pitch angle to the experimental results (pink line). At a collective pitch of 2° (highlighted by a red circle in both figures), the CFD/CSD produced -1.6 lbs of thrust while the experiment recorded -0.5 lbs. Figure 34 represents the power results. Here, the computational power was calculated at 2.06 Hp while the experimental results denote 1 Hp. Dissimilarities between the parameters may be the result of computational grid quality or experimental tare balancing. While the CFD/CSD results are not exactly equivalent to the experiment, the difference between the experimental and computational results remain the same at each change in

collective pitch. Conclusively, the consistent trend in thrust and power validates the CFD and harmonic balancing approach.

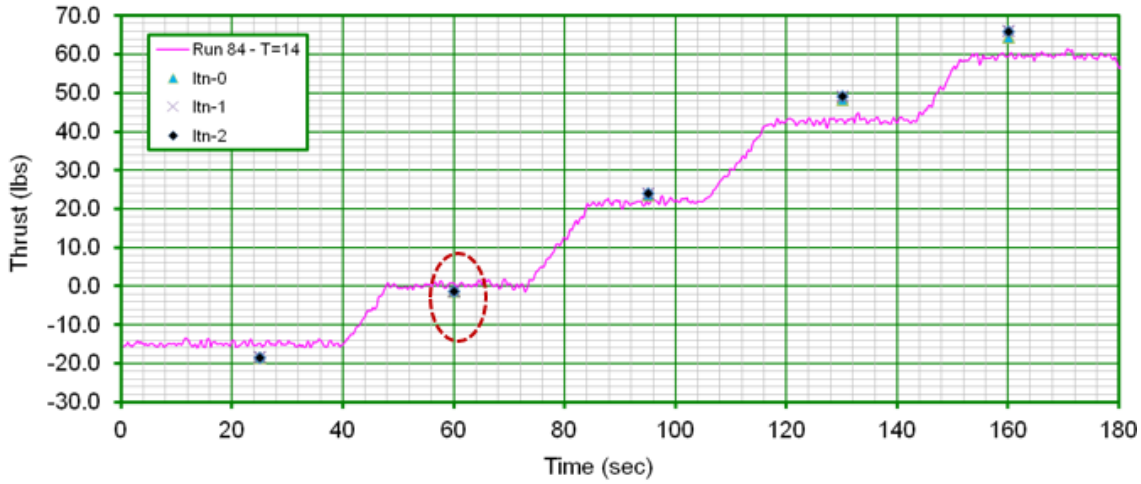

Figure 33: Comparison of experimental thrust values (Case 81) with CFD/CSD results for collective sweep 0°, 2°, 5°, 8°, 10°

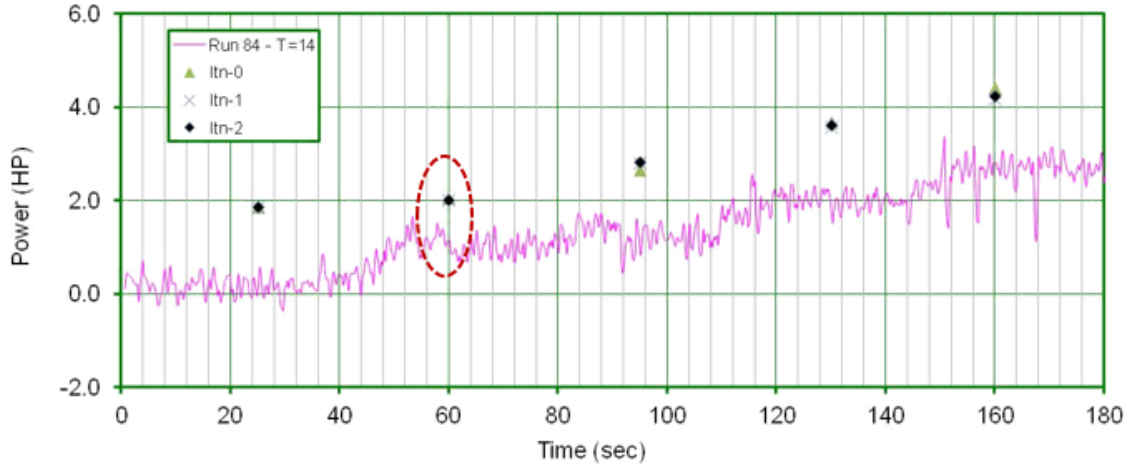

Figure 34: Comparison of experimental power values (Case 81) with CFD/CSD results for collective sweep 0°, 2°, 5°, 8°, 10°

5.4.3 Results

Case 2 represents a condition with the cold ambient temperature of -30°C and a moderate rotor speed of 60kts. Combination of these two parameters will produce rime ice shapes. Figure 37 illustrates the projection blade streamlines onto the xy plane at $\Psi = 0°$.

At this azimuth location, the blade begins to enter the advancing side of the rotor disk. The highly swept nature of the streamlines indicate a large presence of span-wise flow. As such, this azimuth station represents an appropriate test case to assess the ice prediction differences between the new methodology and the original strip theory.

Figure 38 represents the ice prediction results for $\Psi = 0°$ at the selected radial locations 25% R, 37% R, 50% R, 61% R, 74% R, and 86% R. The locations with respect to the blade are illustrated by the pink lines in Figure 37. Each plot in Figure 38 compares the predicted ice shape of the two methodologies. Qualitatively, there is almost no difference between the strip theory results (pink line) and the streamline results (blue line). Near the tip region at 86% R, there is a slight deviation between the two results, but the change in thickness in nominal and the shape retains the smooth rime characteristics.

The results from the other three azimuth locations are provided in Figure 40, Figure 42, and Figure 44. Variations in span-wise strength across the disk did not produce significant differences in ice shape.

The case 53 test condition retains the same advanced ratio as Case 2, but at a warmer ambient temperature and lower collective pitch. This test case was chosen since the warmer temperature will create a more glaze or mixed ice than those produced in Case 2. The creation of more irregular ice shapes might be more sensitive to span-wise flow.

Since the azimuthal sensitivity study performed in Case 2 concluded that span-wise flow strength was not an important factor, ice was only accreted at $\Psi = 0°$. Figure 46 presents the ice prediction results at the selected radial locations 37% R, 50% R, 61% R, 74% R, and 86% R, and 98% R. Similarly to Case 2, the ice shapes are almost exact matches to the strip theory results. In particular, Figure 46f represents the generated ice shape at the blade's tip. The predicted geometry shows the beginning formation of a double horn ice shape, thus categorizing it as glaze ice. Even with the departure from rime ice, streamline and strip theory results remain in agreement.

5.4.4 Discussion

The results of both test conditions conclude that the inclusion of span-wise flow produced nominal changes in ice shape compared to the strip theory predictions throughout the entire rotor disk. Changes in collection pitch angle and ice accretion type did not influence any divergence from the original methodologies results. The severity of the span-wise influence also had no effect. Thus, the strip theory approach remains an appropriate technique for rotor blade ice accretion prediction.

A possible explanation for the lack of influence is because of the surface collection efficiency's characteristics. Due to the water impingement trajectory, majority of droplets will land at the leading edge of the rotor blade with small variations across the span. This characteristic is graphically represented in Figure 35, a contour plot of the collection efficiency across the blade surface for Case 53 at $\Psi = 0°$. Here, it can be seen that very few droplets impinge the blade surface behind the leading edge. Since all streamlines were designated to start at the stagnation point, there is only a slight difference between the collection efficiency used in the strip theory approach and the streamline approach. This is demonstrated by Figure 36. The plot illustrates the chord-wise collection efficiency starting from the lower surface of the trailing and wrapping around the surface at the radial station 61% of the blade span. There is an insignificant difference between the strip theory approach and the span-wise influence approach.

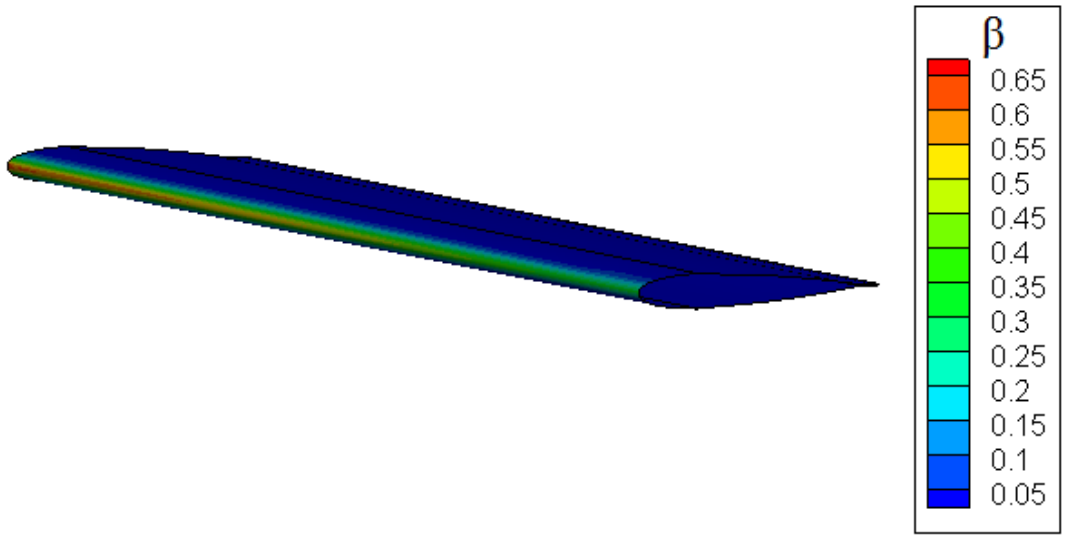

Figure 35: Contour plot of collection efficiency for Case 53 at Ψ = 0°

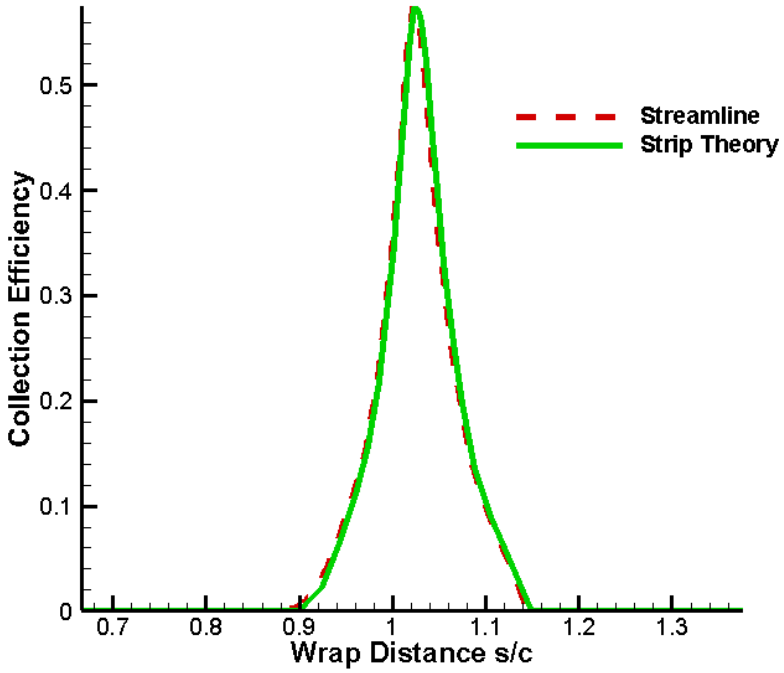

Figure 36: Collection efficiency at 61%R for Case 53 Ψ= 0°

CHAPTER 6

CONCLUSIONS

6.1 Summary

The formation of in-flight icing causes significant performance degradation for rotorcraft. To maintain safe levels of handling qualities in flights intercepting icing environments, manufacturers must comply with stringent icing certification regulations. This thesis work presents a synopsis of the current state of in-flight icing and argues that research focused on improving numerical ice shape prediction is essential to the future of icing certification. The thesis also discusses a new methodology to predict ice shapes on rotor blades.

The document begins by discussing the process of in-flight ice accretion. There are three main categories of ice; rime, glazed and mixed. The type of ice shape is determined by surrounding environment's atmospheric parameters and the geometry of the vehicle. Chapter 2 also lists the different levels of icing certification in the United States, United Kingdom and the European Union. The first level restricts all flights into known icing conditions. The second allows limited in-flight icing and is only allotted for specific helicopters in the UK. The third certification level allows flights into known icing conditions by requiring a full suite of onboard ice protection systems.

An analysis on the popularity of icing certification is provided in Chapter 3. The results indicate the process required to obtain certification is relatively undesirable to manufacturers. Currently, most helicopters are not certified for flight into known icing conditions. Even operations which frequently experience icing environments do not utilize helicopters outfitted with the appropriate ice protection technology. Without certification, flights are restricted to operational envelopes clear of potential and known icing environments. The main consequences of this limitation result in the disregard of

regulations by aircrews and the obstruction of mission success. Investigations interviewing military and civilian rotorcraft aircrews found a widely held opinion that mission operations and aircrew safety would benefit from helicopters certified with limited icing clearance.

In response to the need of rotorcraft operators and manufacturers, research focused on the improving the numerical ice accretion prediction is essential. Since flight testing and tunnel testing are limited to a certain range of achievable test conditions, the main benefit of using computational solvers to supplement certification compliance stems from the ability of icing software to test a much broader range of conditions.

Chapter 4 outlines the process of numerically predicting ice accretion. The general methodology involves four distinct modules; (1) flow field calculation, (2) water droplet impingement characteristics, (3) thermodynamics of ice accretion, and (4) calculation of resulting ice shapes. LEWICE, the accredited ice prediction code, internally calculates the four modules. However, a modification of LEWICE was created to externally compute modules (1) and (2) in order to increase the fidelity of ice predictions. Validation cases conclude the modified sequence produces accurate ice shapes.

Building from the technique presented in Chapter 4, a new approach to three dimensional icing predictions is proposed in Chapter 5. The objective of the modified process is to include the influence of span-wise flow within LEWICE's thermodynamic module and the subsequence prediction of ice accretion. The new approach includes span-wise flow by computing the coefficient of pressure and collection efficiency along a blade's surface streamlines. Chapter 5 details the multiple steps required to calculate the streamline locations and the process of interpolating the final ice shape.

Before completing this research effort, it was theorized that the strip theory based approach was more suitable for ice analysis on fixed wing aircraft since rotor blades consistently experience span-wise flow due to flow separation and/or centrifugal forces as it traverses around the rotor disk. The results from two test cases, with varying temperature

and collective pitch angle, indicate that the inclusion of span-wise flow has no effect on the predicted ice shape. It is hypothesized the insensitivity to span-wise flow is due to water droplets mainly impacting the surface at the leading edge. Thus, creating similar collection efficiency profiles between the streamline approach and the classical approach.

Although the streamline methodology did not enhance accuracy of predicted ice shapes as previously believed, it is now confirmed the original strip theory is an appropriate method for rotor blades.

6.2 Further Research

Expansions to this research would involve code validation with experimental results. Mentioned in Section 5.4, the test conditions were pulled from a recent icing tunnel experiment performed on a Bell 206 tail rotor system. Using the test's 3-D ice scans, the resulting shapes can be compared to the experimental results. Since the tunnel tests accrete ice for over three minutes, completion of this task must utilize the multi-step version of the proposed ice accretion process. It has been found that LEWICE's prediction accuracy decreases when time step periods are over one minute.

A multi-step process implies that the blade surface mesh must be regenerated after every step. Currently, no method was formulated to grid the iced blade surface. The tools employed in this research effort require a structured surface mesh to hyperbolically generate the C-H volume grid. Since new information of blade geometry is only stored along the curved surface streamlines, the complexity of generating a structured surface mesh quickly increases. One proposed method recreates the surface by triangulating the spaces between streamline and interpolating points at the appropriate radial locations. Another method enlists the use of radial basis functions (RBF), a type of surrogate modeling. RBFs are real-valued functions which find information at desired locations by training a model based on the distances between the original values.

Future research should also focus on analyzing runback refreeze with the span-wise influence approach. Although ice accretion was independent of span-wise flow, the runback refreeze phenomena may be more sensitive. Runback refreeze is a process caused by the presence of anti-icing or de-icing systems. As a heating element melts formed ice or forces impinging droplets to remain in a liquid state, the resulting water will run back along the blade due to inertial and aerodynamic forces. As the water retreats behind the leading edge heaters, it may refreeze to the surface behind the heater. The new formation of ice causes performance degradation and cannot be effectively removed by leading edge heaters since it is formed farther back on the blade surface. It is postulated that the runback water will most likely follow the streamline path. If this proves true, then the refreezing of ice may occur at different locations than predicted by the classical strip theory approach.

In addition, researching ways to increase the methodology's automation is highly beneficial. Currently, the process is highly labor intensive. Manually finding the streamline locations with Tecplot360 decreases the usability of the new methodology. A script computing the streamline locations and the corresponding flow field information with techniques similar to Tecplot360 would decrease the required user interaction and the total computation time.

Finally, the methodology to predict ice accretion is highly module. As such, it has the ability to implement different technologies such as commercial programs like NASA's CFD software OVERFLOW. The methodology also has potential to be used within the Helios platform. Helios is an intermediate-level software infrastructure that links existing software modules with little need for extensive code modifications. With Helios, ice accretion can be performed in conjunction with full rotorcraft body calculations.

APPENDIX

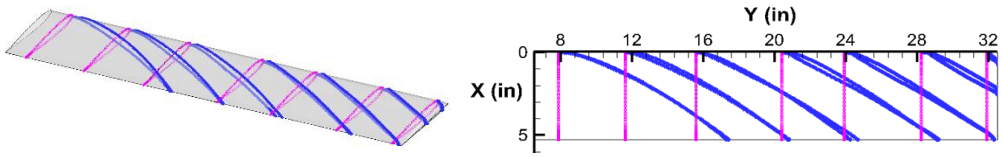

Figure 37: Illustration of Case 2 streamlines at selected radial locations for azimuth = 0°

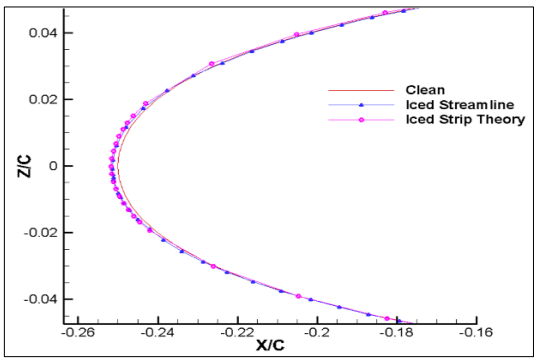

a) Radial = 8”

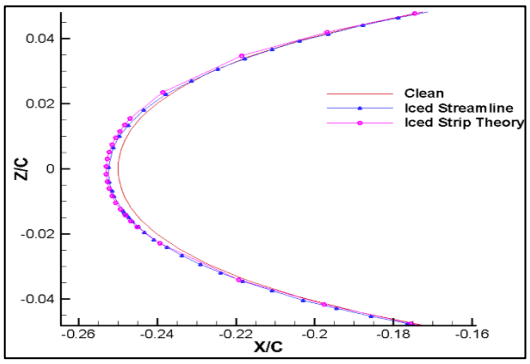

b) Radial = 12”

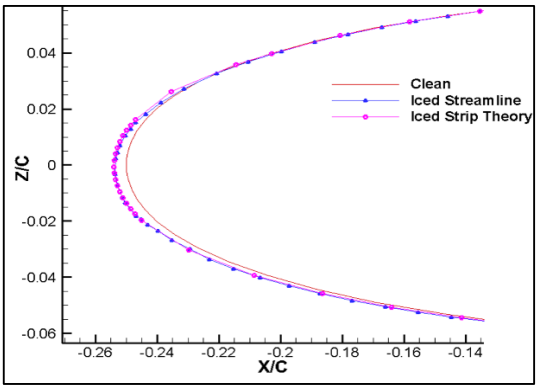

c) Radial = 16”

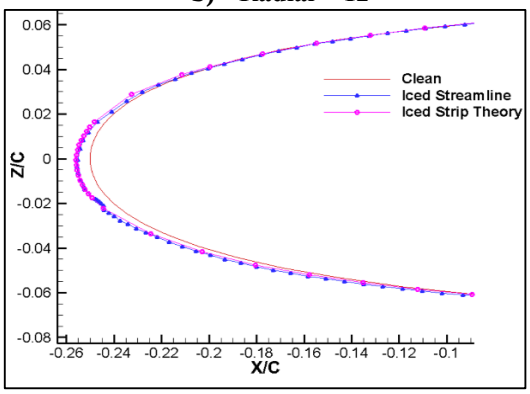

d) Radial = 20”

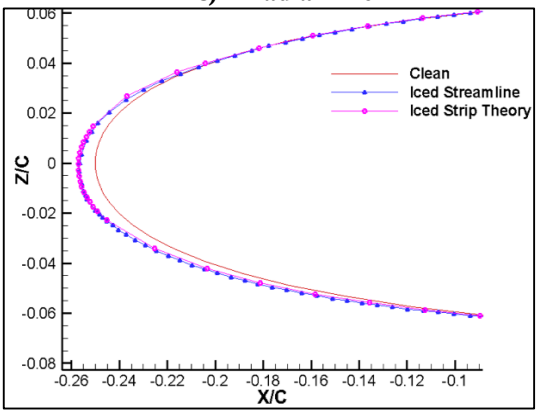

e) Radial = 24”

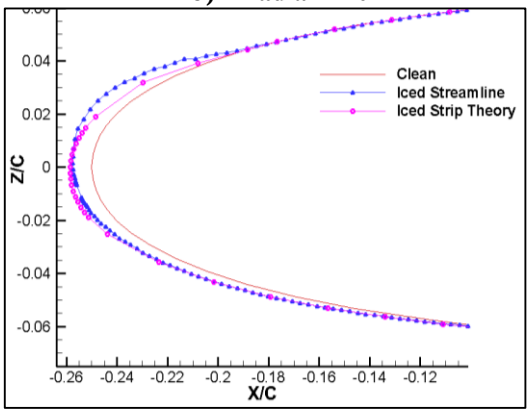

f) Radial = 28”

Figure 38: Results of Case 2 ice prediction at Ψ=0° Comparison of calculated ice shaped using the streamline approach and the original strip theory approach at radial locations a) 8”, b) 12”, c) 16”, d) 20”, e) 24”, and f) 28”

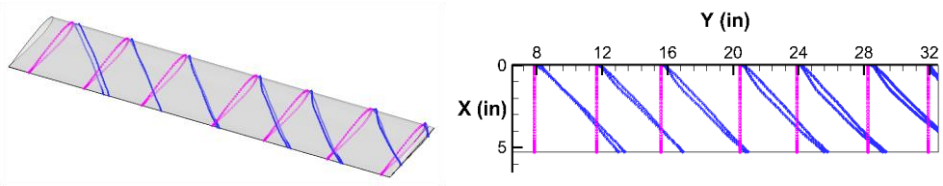

Figure 39: Illustration of Case 2 streamlines at selected radial locations for azimuth = 90°

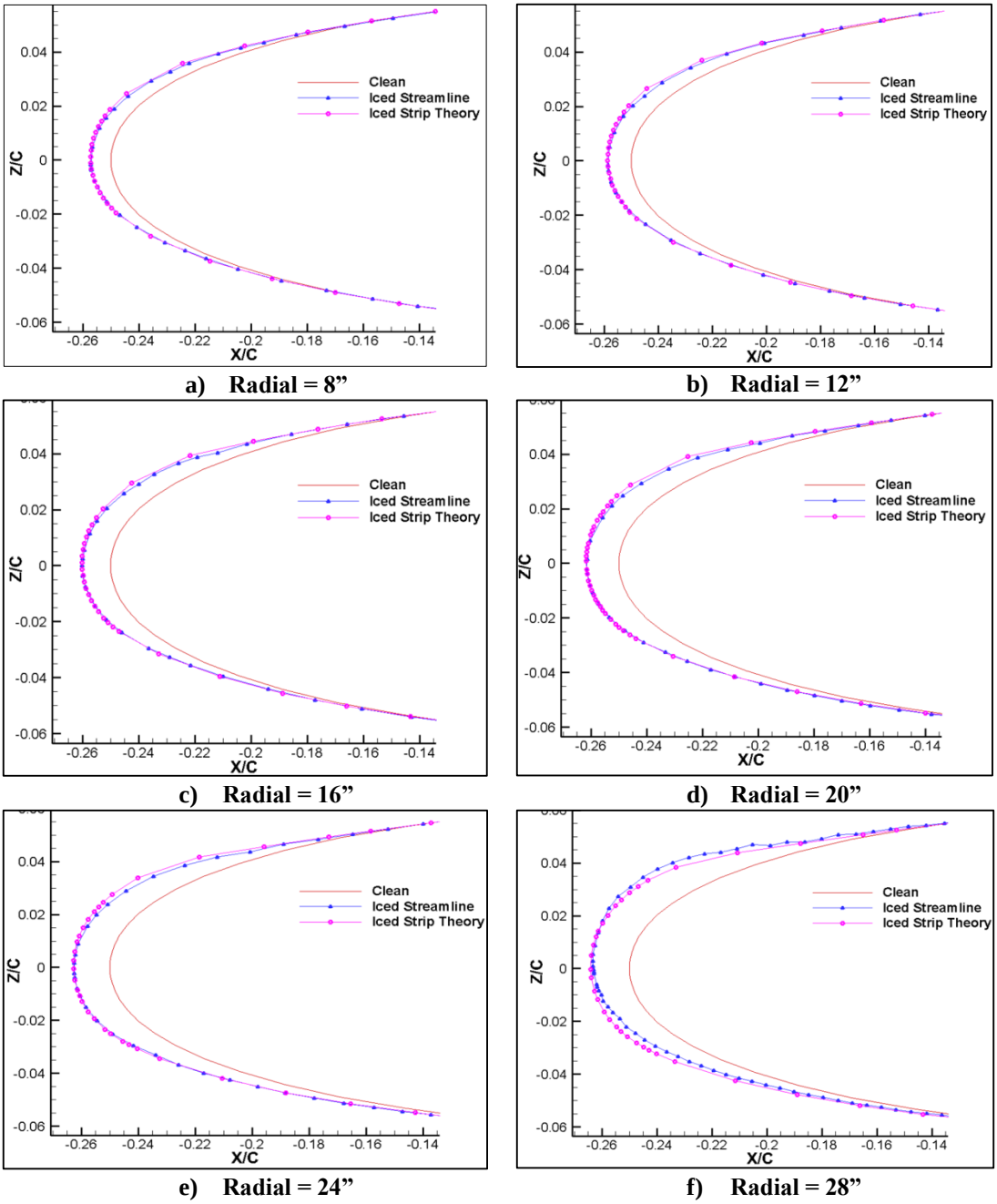

a) Radial = 8”

b) Radial = 12”

c) Radial = 16”

d) Radial = 20”

e) Radial = 24”

f) Radial = 28”

Figure 40: Results of Case 2 ice prediction at Ψ=90° Comparison of calculated ice shaped using the streamline approach and the original strip theory approach at radial locations a) 8”, b) 12”, c) 16”, d) 20”, e) 24”, and f) 28”

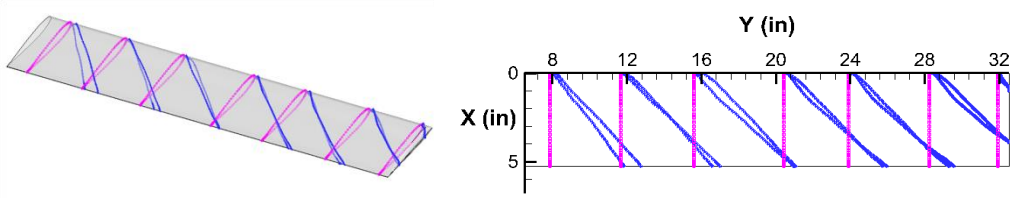

Figure 41: Illustration of Case 2 streamlines at selected radial locations for azimuth = 180°

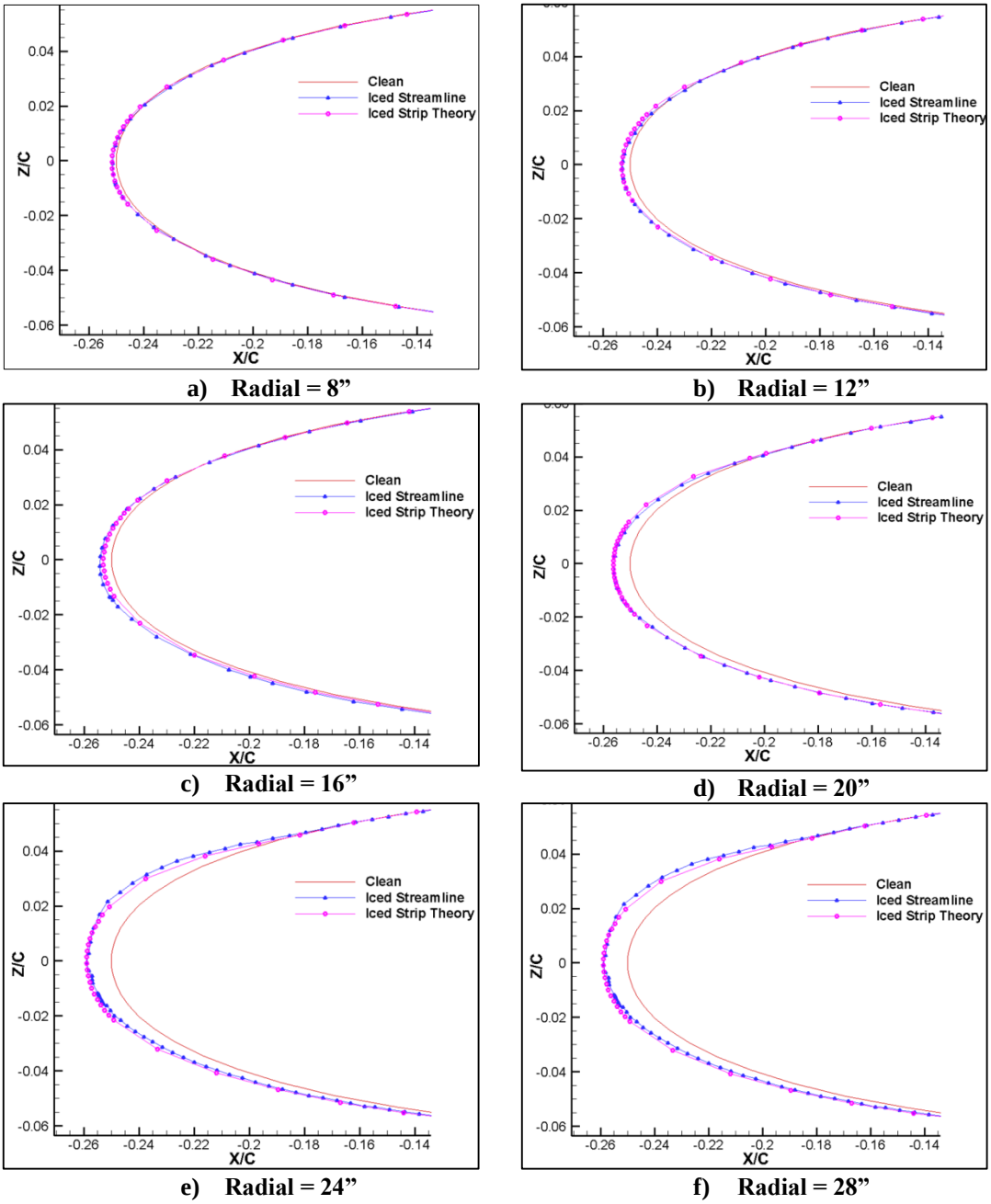

a) Radial = 8”

b) Radial = 12”

c) Radial = 16”

d) Radial = 20”

e) Radial = 24”

f) Radial = 28”

Figure 42: Results of Case 2 ice prediction at Ψ=180° Comparison of calculated ice shaped using the streamline approach and the original strip theory approach at radial locations a) 8”, b) 12”, c) 16”, d) 20”, e) 24”, and f) 28”

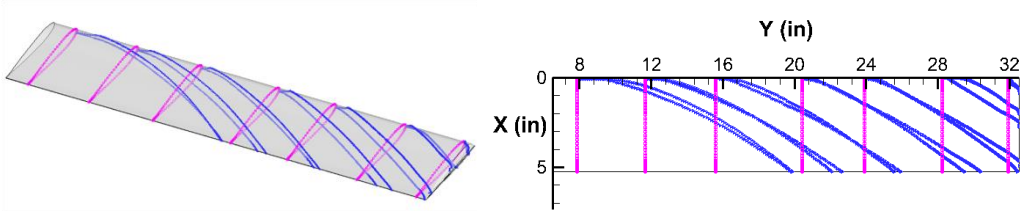

Figure 43: Illustration of Case 2 streamlines at selected radial locations for azimuth = 270°

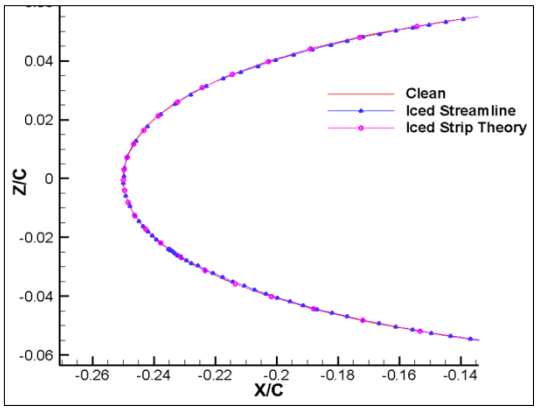

a) Radial = 8”

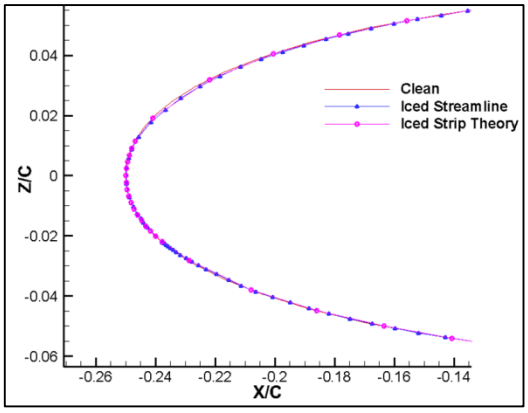

b) Radial = 12”

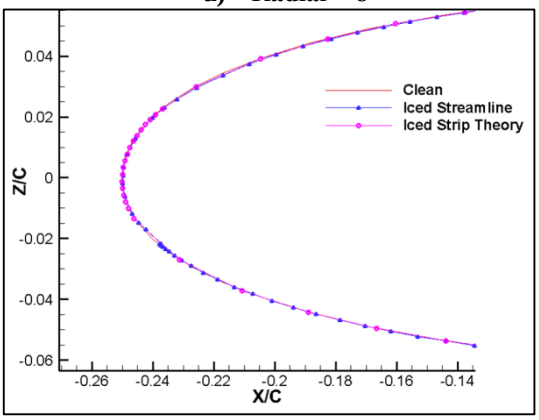

c) Radial = 16”

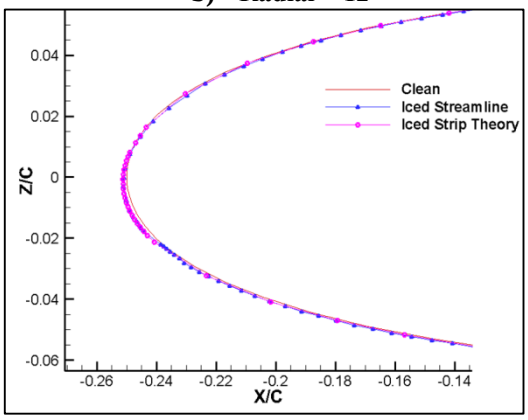

d) Radial = 20”

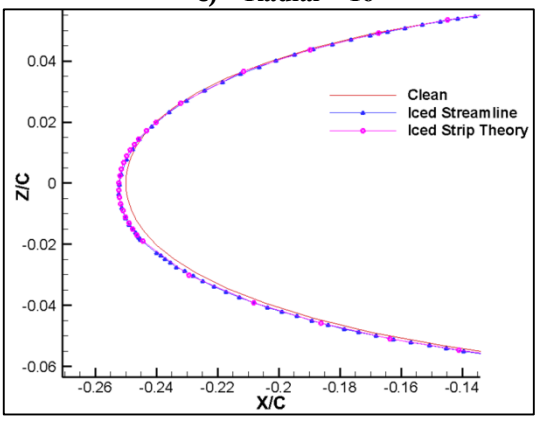

e) Radial = 24”

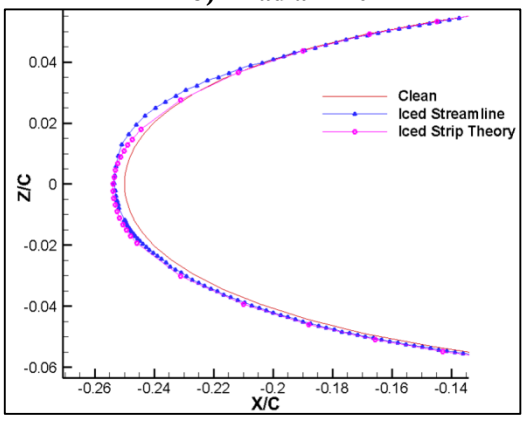

f) Radial = 28”

Figure 44: Results of Case 2 ice prediction at Ψ=270° Comparison of calculated ice shaped using the streamline approach and the original strip theory approach at radial locations a) 8”, b) 12”, c) 16”, d) 20”, e) 24”, and f) 28”

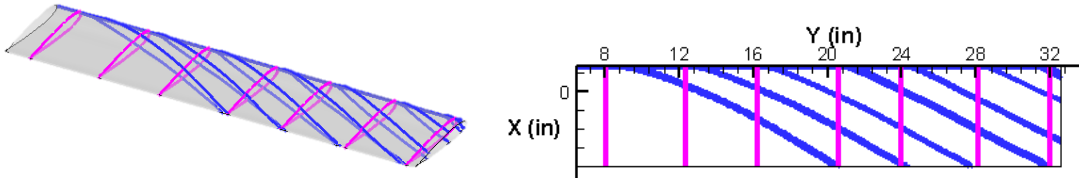

Figure 45: Illustration of Case 53 streamlines at selected radial locations for azimuth = 0°

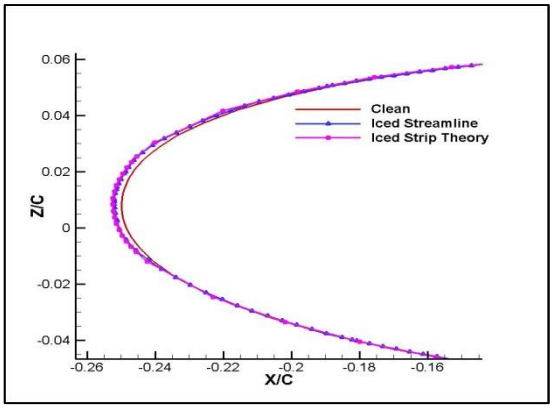

a) Radial = 12”

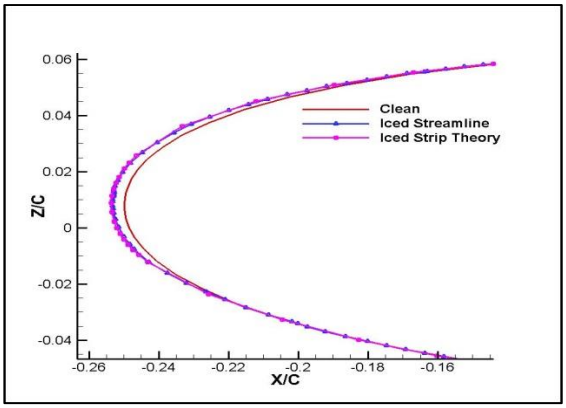

b) Radial = 16”

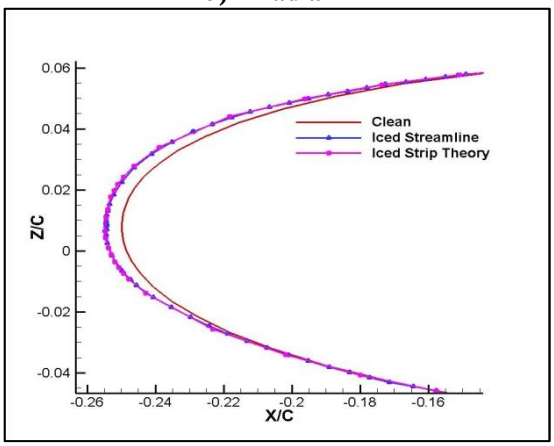

c) Radial = 20”

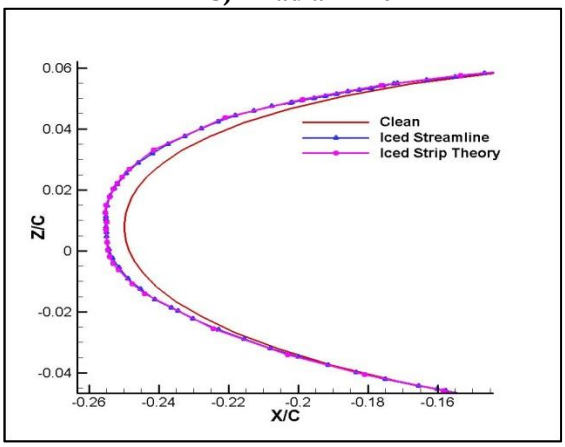

d) Radial = 24”

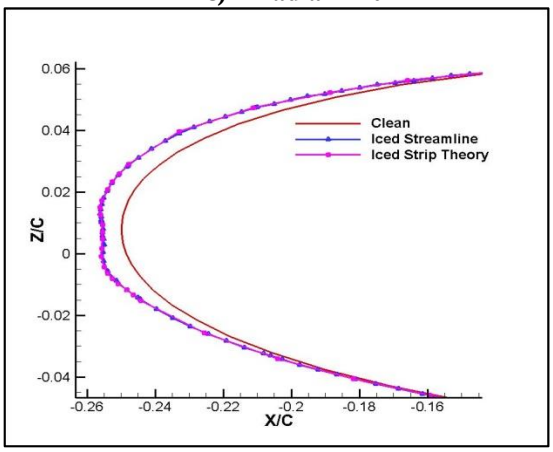

e) Radial = 28”

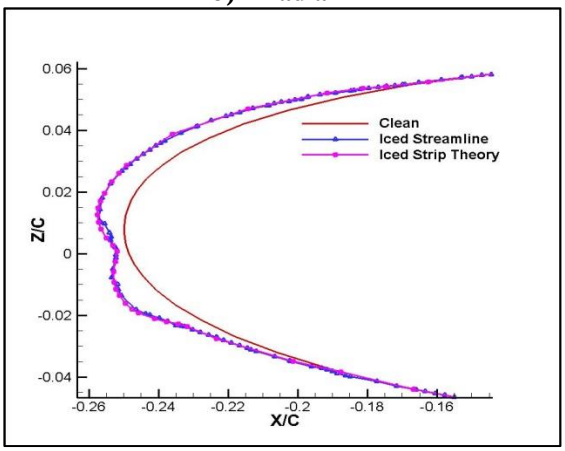

f) Radial = 32”

Figure 46: Results of Case 53 ice prediction at Ψ=0° Comparison of calculated ice shaped using the streamline approach and the original strip theory approach at radial locations a) 12”, b) 16”, c) 20”, d) 24”, e) 28”, and f) 32”

REFERENCES

[1] Federal Aviation Administration, "Fact Sheet- FAA & NTSB "Most Wanted" Recommendations," 2010.

[2] T. L. Miller and T. H. Bond, "Icing Tesearch Tunnel test of a model helicopter rotor," in *AHS 45th Annual Forum*, Boston, MA, March 22-24, 1989.

[3] R. J. Flemming, R. K. Britton and T. H. Bond, "Model rotor icing tests in the NASA Lewis Icing Research Tunnel," NASA, April 1991.

[4] R. J. Flemming, "Icing tests of UH-60A/L rotor blade erosion coatings in the NASA Glenn Research Center Icing Research Tunnel," October 2005.

[5] R. J. Flemming and A. Saccullo, "Tests of a model main rotor in the NASA Lewis Research Center Icing Research Tunnel," NASA, January 1991.

[6] R. J. Flemming, T. H. Bond and R. K. Britton, "Results of a sub-scale model rotor icing test," in *AIAA 29th Aerospace Sciences Meeting*, January 1991.

[7] R. K. Britton, T. H. Bond and R. J. Flemming, "An overview of a model rotor icing tests in the NASA Lewis Icing Research Tunnel," NASA, Cleveland, January 1994.

[8] R. J. Flemming and D. A. Lednicer, "High speed ice accretion on rotor airfoils," NASA, Noermber 1984.

[9] R. J. Flemming, R. K. Britton and T. H. Bond, "Role of wind tunnels and computer codes in the certification and qualification of rotorcraft for flight in forecast icing," NASA, Cleveland, October 1994.

[10] W. B. Wright, "Validation results for LEWICE 3.0," in *AIAA 43rd Aerospace Sciences Meeting and Exhibit*, Reno, NV, January 2005.

[11] "Meteorology - Part II," [Online]. Available: http://www.langleyflyingschool.com/Pages/CPGS%20Meteorology,%20Part%202.html#_ftnref1. [Accessed December 2013].

[12] "Fact Sheet- Flying in icing conditions," Federal Aviation Administration, 2010.

[13] M. G. Potapzcuk, "Aircraft icing research at NASA Glenn Research Center," *Journal of Aerospace Engineering*, vol. 26, no. 2, pp. 260-276, April 2013.

[14] *Airworthiness Standards: Transport category rotorcraft*, Federal Aviation Administration, September 1999.

[15] M. K. Politovich, "Aircraft icing," pp. 68-75, 2003.

[16] "Large Rotorcraft," Joint Aviation Authorities, November 1993.

[17] "Recommendations for rotorcraft during icing/snowy conditions," Federal Aviation Administration, January 20113.

[18] "Advisory material for helicopter limited icing clearance," Civil Aviation Authority, London, 1996.

[19] "Inflight icing and the helicopter," *Helicopter Safety*, vol. 16, no. 6, Nov/Dec 1990.

[20] L. Peck, C. C. Ryerson and C. J. Martel, "Army aircraft icing," U.S Army Cold Regions Research and Engineering Lab, Hanover, NH, September 2002.

[21] M. Davis, "Helicopter Operations: The icing factor," vol. 4, November 2007.

[22] M. P. Simpson and P. M. Render, "Certification and operation of helicopters in icing environments," in *AIAA 35th Aerospace Sciences Meeting*, Reno, NV, January 6-9, 1998.

[23] S. D. Green, "A study of U.S. inflight icing accidents and incidets, 1978-2002," in *44th AIAA Aerospace Sciences Meeting and Exhibit*, Reno, NV, January 9-12, 2006.

[24] W. B. Wright and A. Rutkowski, "Validation results for LEWICE 2.0," NASA, January 1999.

[25] T. Hedde and D. Guffond, "ONERA three-dimensional icing model," *AIAA Journal*, vol. 33, no. 6, pp. 1038-1045, 1995.

[26] C. N. Aliaga, M. S. Aube and G. S. Baruzzi, "FENSAP-ICE-Unsteady: Unified in-flight icing simulation methodology for aircraft, rotorcraft, and jet engines," *Journal of Aircraft*, vol. 48, no. 1, pp. 119-126, Jan/Feb 2011.

[27] S. Gouttebroze, F. Saeed and I. Paraschivoiu, "CANICE- Capabilities and current status," in *NATAO/RTO Workshop, Assessment of icing code prediction capabilities*, CIRA, Capua, Italy, December 2000.

[28] W. B. Wright, "User manual for the NASA Glenn ice accretion code LEWICE: Version 2.0," National Aeronautics and Space Administration, Cleveland, OH, 1999.

[29] J. L. Hess and A. M. O. Smith, "Calculation of potential flow about arbitrary bodies," *Progress in Aeronautical Sciences,* vol. 8, pp. 1-138, 1967.

[30] W. Frost, H. Chang, C. Shieh and K. Kimble, "Two-dimensional particle trajectory computer program," Interim Report for Contract NAS3-22448, 1982.

[31] B. L. Messigner, "Equilibrium Temperature of an unheated icing surface as a funciton of airspeed," *Journal of the Aeronautical Sciences,* vol. 20, pp. 29-42, 1953.

[32] H. Beaugendre, F. Morency and W. Habashi, "Development of a second generation in-flight icing simulation code," *Journal of Fluids Engineering,* vol. 128, no. 2, pp. 378-387, March 2006.

[33] B. Y. Min and L. N. Sankar, "Enhancements of a hybrid Navier-Stokes/free wake method for improved prediction of blade-vortex interaction phenomena," in *AIAA 27th Applied Aerodynamics Conference,* San Antonio, TX, June 2009.

[34] B. Y. Min, W. Lee, R. Englar and L. N. Sankar, "Numerical invesitigation of ciruclation control airfoils," *Journal of Aircraft,* vol. 46, no. 4, pp. 1403-1410, 2009.

[35] M. Nucci, J. Bain and L. N. Sankar, "Assessment of the effects of computational parameters on physics-based models of ice accretion," in *AIAA 48th Aerospace Sciences Meeting*, Orlando, FL, January 2010.

[36] M. H. Beaugendre and W. D. Habashi, "FENSAP-ICE's three dimensional in-flight ice accretion module - ICE3D," *Journal of Aircraft,* vol. 40, no. 2, pp. 239-247, 2003.

[37] J. W. Kim, D. P. Garza and L. N. Sankar, "Ice accretion modeling using an Eulerian approach for droplet impingement," in *AIAA 51st Aerospace Sciences Meeting*, Grapevine, TX, January 2013.

[38] R. K. Britton and T. H. Bond, "A review of ice accretion data from a model rotor icing test and comparison with theory," in *AIAA 29th Aerospace Sciences Meeting*, Reno, NV, January 1991.

[39] K. Korkan, L. Dadone and R. Shaw, "Performance degradation of helicopter rotor systems in forward flight due to ice," *Journal of Aircraft,* vol. 22, no. 8, pp. 713-718, August 1985.

[40] E. W. Brouwers, J. L. Palacios and E. C. Smith, "The experimental investigation of a rotor hover icing model wih shedding," in *AHS 66th Annual Forum*, Phoenix, AZ, May 11-13, 2010.

[41] R. H. Johnson, "An evaluation of the HpH 304C Wasp standard class sailplane," 30 December 2002. [Online]. Available: http://www.wingsandwheels.com/Johnson%20test.htm.

[42] W. M. Chan, "The OVERGRID interface for computaional simulations on overset grids," in *AIAA 32nd Fluid Dynamics Conference*, St. Louis, MO, June 2002.

[43] N. Rajmohan, L. N. Sankar, O. Bauchau, B. Charles, S. Makinen and T. A. Egolf, "Application of hybrid methodology to rotors in steady and maneuvering flight," in *AHS 64th Annual Forum*, 2008.

[44] Tecplot Support, "Streamtrace calculation," 24 September 2009. [Online]. Available: http://www.tecplot.com/knowledgebase/2009/09/24/streamtrace-calculation/.